density to alendronate in postmenopausal Japanese women with osteoporosis. J Bone Miner Metab 23:238–242
34. Garnero P, Dargent-Molina P, Hans D, Schott AM, Breart G, Meunier PJ, Delmas PD (1998) Do markers of bone resorption add to bone mineral density and ultrasonographic heel measurement for the prediction of hip fracture in elderly women? The EPIDOS prospective study. Osteoporos Int 8:563–569
35. Kung AW, Yeung SS (1996) Prevention of bone loss induced sby thyroxine suppressive therapy in postmenopausal women: the effect of calcium and calcitonin. J Clin Endocrinol Metab 81:1232–1236
36. Akcay MN, Akcay G, BIlen H (2004) The effect of calcitonin on bone resorption in hyperthyroidism: a placebo-controlled clinical study. J Bone Miner Metab 22:90–93
37. Cummings SR, Karpf DB, Harris F, Genant HK, Ensrud K, LaCroix AZ, Black DM (2002) Improvement in spine bone density and reduction in risk of vertebral fractures during treatment with antiresorptive drugs. Am J Med 112:281–289
38. Rosen CJ, Hochberg MC, Bonnick SL, McClung M, Miller P, Broy S, Kagan R, Chen E, Petruschke RA, Thompson DE, de Papp AE (2005) Fosamax Actonel Comparison Trial Investigators. Treatment with once-weekly alendronate 70 mg compared with once-weekly risedronate 35 mg in women with postmenopausal osteoporosis: a randomized double-blind study. J Bone Miner Res 20:141–151
39. Reginster J, Minne HW, Sorensen OH, Hooper M, Roux C, Brandi ML, Lund B, Ethgen D, Pack S, Roumagnac I, Eastell R (2000) Randomized trial of the effects of risedronate on vertebral fractures in women with established postmenopausal osteoporosis. Vertebral Efficacy with Risedronate Therapy (VERT) Study Group. Osteoporos Int 11:83–91
40. Hamilton B, McCoy K, Taggart H (2003) Tolerability and compliance with risedronate in clinical practice. Osteoporos Int 14:259–262

Diabetologia (2006) 49: 962–968
DOI 10.1007/s00125-006-0193-8

ARTICLE

T. Tomita · H. Masuzaki · H. Iwakura · J. Fujikura · M. Noguchi · T. Tanaka · K. Ebihara · J. Kawamura · I. Komoto · Y. Kawaguchi · K. Fujimoto · R. Doi · Y. Shimada · K. Hosoda · M. Imamura · K. Nakao

Expression of the gene for a membrane-bound fatty acid receptor in the pancreas and islet cell tumours in humans: evidence for GPR40 expression in pancreatic beta cells and implications for insulin secretion

Received: 3 August 2005 / Accepted: 23 December 2005 / Published online: 9 March 2006

Abstract *Aims/hypothesis* G protein-coupled receptor 40 (GPR40) is abundantly expressed in pancreatic beta cells in rodents, where it facilitates glucose-induced insulin secretion in response to mid- to long-chain fatty acids in vitro. However, *GPR40* gene expression in humans has not been fully investigated, and little is known about the physiological and pathophysiological roles of GPR40 in humans. The aim of this study, therefore, was to examine GPR40 expression and its clinical implications in humans. *Methods: GPR40* mRNA expression in the human pancreas, pancreatic islets and islet cell tumours was analysed using TaqMan PCR. *Results: GPR40* mRNA was detected in all human pancreases collected intraoperatively. It was enriched approximately 20-fold in isolated islets freshly prepared from the pancreases of the same individuals. The estimated mRNA copy number for the *GPR40* gene in pancreatic islets was comparable to those for genes encoding sulfonylurea receptor 1, glucagon-like peptide 1 receptor and somatostatin receptors, all of which are known to be expressed abundantly in the human pancreatic islet. A large amount of *GPR40* mRNA was detected in insulinoma tissues, whereas mRNA expression was undetectable in glucagonoma or gastrinoma. The *GPR40* mRNA level in the pancreas correlated with the insulinogenic index, which reflects beta cell function (r=0.82, p=0.044), but not with glucose levels during the OGTT, the insulin area under the OGTT curve or the index for the homeostasis model assessment of insulin resistance (HOMA-IR). *Conclusions/interpretation* The present study provides evidence for *GPR40* gene expression in pancreatic beta cells and implicates GPR40 in insulin secretion in humans.

Keywords Human · GPR40 · Pancreas · Pancreatic islets · Insulinoma · Insulin secretion

Abbreviations GLP1R: glucagon-like peptide 1 receptor · GPR40: G protein-coupled receptor 40 · GSIS: glucose-stimulated insulin secretion · HOMA-IR: homeostasis model assessment of insulin resistance · SSTR: somatostatin receptor · SUR1: sulfonylurea receptor 1

T. Tomita · H. Masuzaki (✉) · H. Iwakura · J. Fujikura · M. Noguchi · T. Tanaka · K. Ebihara · K. Hosoda · K. Nakao
Department of Medicine and Clinical Science,
Kyoto University Graduate School of Medicine,
54 Shogoin Kawahara-cho, Sakyo-ku,
Kyoto 606-8507, Japan
e-mail: hiroaki@kuhp.kyoto-u.ac.jp
Tel.: +81-75-751-3172
Fax: +81-75-771-9452

J. Kawamura · I. Komoto · Y. Kawaguchi · K. Fujimoto · R. Doi · Y. Shimada · M. Imamura
Department of Surgery and Surgical Basic Science,
Kyoto University Graduate School of Medicine,
Kyoto, Japan

Introduction

Fatty acids play a pivotal role in a variety of metabolic controls and cell signalling processes in various tissues [1]. In particular, short-term exposure of fatty acids to pancreatic beta cells augments glucose-stimulated insulin secretion (GSIS), a process in which fatty acid-derived metabolites such as long-chain fatty acyl-CoAs act as crucial effectors [2]. However, the entire mechanism whereby fatty acids acutely induce GSIS augmentation has not been fully elucidated [3]. In contrast, chronic fatty acid exposure causes marked deterioration of beta cell function, which is referred to as lipotoxicity [4, 5].

Several investigators have recently demonstrated that fatty acids act as ligands for membrane-bound G-protein-coupled receptors such as GPR40 [3, 6, 7], GPR41, GPR43 [8, 9] and GPR120 [10]. GPR40 is preferentially expressed in pancreatic beta cells in rodents and augments GSIS after acute exposure to mid- and long-chain fatty acids [6]. Silencing GPR40 with the small interfering RNA (siRNA) system suppresses long-chain fatty acid-induced GSIS augmentation in pancreatic beta cells [6]. A recent study of

GPR40 knockout mice and beta-cell-specific GPR40 transgenic mice suggested a physiological and pathophysiological role for GPR40 in insulin secretion and diabetes mellitus [11]. Although these findings implicate GPR40 in insulin secretion and glucose metabolism in rodents, little is known about the physiological significance of GPR40 in humans.

In this context, we investigated *GPR40* gene expression in the pancreas and in islet cell tumours collected during surgery. We also explored the potential role of GPR40 in beta cell function in humans.

Subjects and methods

Participants, tissue sampling and pancreatic islet preparation

Seventeen patients with pancreatic tumours provided written informed consent to participation in the present study, which was approved by the Ethical Committee on Human Research of Kyoto University Graduate School of Medicine (No. 508, 2003), and conducted according to the principles of the Declaration of Helsinki. Table 1 summarises the patient profiles. Patients who underwent pancreatectomy (patients 1–12) were numbered according to the *GPR40* mRNA level in the pancreas. None of the 12 patients were treated with oral glucose-lowering agents or insulin. Pancreatic, intestinal and hepatic tissues free of tumour invasion as well as islet cell tumour tissues were obtained at the time of surgery (Table 1). Islet tissues from three patients (patients 9–11) were promptly isolated from the pancreas through the mince method [12]. Briefly, the pancreas was finely minced by hand for 15–30 min on ice and digested at 37°C with 600 IU/ml of type V collagenase (Sigma, St Louis, MO, USA) in Hanks' Balanced Salt Solution (HBSS) containing 1% bovine serum albumin (Fraction V, Sigma) for 20 min. The digested tissue was washed three times in cold HBSS. After dithizone staining, pancreatic islets were manually collected using a stereo microscope (SZ-STB1; Olympus, Tokyo, Japan).

Quantification of mRNA expression of *GPR40* and other receptor genes

We measured mRNA expression of the *GPR40* gene as well as genes encoding sulfonylurea receptor 1 (*ABCC8*, previously known as *SUR1*) [13], glucagon-like peptide 1 receptor (*GLP1R*) [14, 15] and somatostatin receptor (*SSTR*) 3 and 5 [16] using the following method. Total RNA was extracted using the Qiagen RNeasy Mini Kit (Qiagen, Hilden, Germany) [17]. First-strand cDNA was synthesised by random hexamer-primed reverse transcription using SuperScript II reverse transcriptase (Invitrogen, Carlsbad, CA, USA) [18]. The mRNA level was quantified by the TaqMan PCR method using an ABI Prism 7700 Sequence Detector (Applied Biosystems, Foster City, CA, USA) as described [19]. To calculate the copy number of each mRNA, standard curves were generated using synthesised oligo DNA fragments (Proligo Japan, Kyoto, Japan) containing the PCR amplicon region. The mRNA expression in each gene was normalised to that of *GAPDH* (i.e. the mRNA level for each gene was expressed as

Table 1 Clinical profiles of patients and tissues

Patient number	Age (years)	Sex (M/F)	Disease	Tissue analysed
1	53	F	Pancreatic cancer	Pancreas (head)/duodenum
2	47	F	Pancreatic cancer	Pancreas (head)/jejunum
3	71	F	Pancreatic cancer	Pancreas (body)
4	59	F	Insulinoma	Pancreas (head)/insulinoma
5	72	F	Pancreatic cancer	Pancreas (head)/jejunum
6	75	M	Pancreatic cancer	Pancreas (head)/duodenum/jejunum
7	45	M	Gastrinoma	Pancreas (body)
8	63	F	Islet cell tumour (non-functional)	Pancreas (body)
9	60	M	Pancreatic cancer	Pancreas (body)
10	63	M	Pancreatic cancer	Pancreas (head)
11	54	M	Pancreatic cancer	Pancreas (head)
12	55	F	Pancreatic cancer	Pancreas (body)
13	64	F	Liver metastasis (glucagonoma)	Liver
14	54	F	Insulinoma	Insulinoma
15	30	M	Insulinoma	Insulinoma
16	23	F	Glucagonoma	Glucagonoma
17	56	M	Gastrinoma	Gastrinoma

Patients were premedicated with 0.01 mg/kg atropine sulphate i.m. and 0.2 mg/kg diazepam orally before surgery
Tissues were sampled under general anaesthesia with 35% O_2, 65% N_2O and 0.5–1.5% sevoflurane. Neuromuscular blockade was provided with vecuronium bromide; initial dose 0.1 mg/kg, supplemented as required

receptor/*GAPDH* [copy/copy]). Table 2 summarises the sequences of primers and probes used in the present study. The primers or probes were designed not to cover any reported single-nucleotide polymorphisms [20–23].

Data analysis on glucose homeostasis

The insulin AUC was calculated using the trapezoidal rule from OGTT data. We evaluated beta cell function and systemic insulin resistance using the insulinogenic index (n=7) and the homeostasis model assessment of insulin resistance (HOMA-IR) (n=10), respectively. The insulinogenic index was calculated as the ratio of the insulin concentration (pmol/l) increment to the glucose concentration (mmol/l) increment at 30 min into the OGTT (Δ30insulin/Δ30glucose) [24]. HOMA-IR was calculated in fasting conditions as plasma insulin (pmol/l)×blood glucose (mmol/l)/22.5 [25, 26]. The difference in the patient numbers for the two indices is based on the difference in data availability, such as blood glucose and insulin levels at 30 min during the OGTT.

Statistical analysis

The relationship between the *GPR40* mRNA level in the pancreas and clinical or metabolic profiles was tested using Spearman's rank correlation and a p value of less than 0.05 was considered significant. The statistical significance of differences in two groups was assessed using unpaired two-tailed t-test and a p value of less than 0.05 was considered significant (Statcel, Social Research Information, Tokyo, Japan).

Results

Expression of *GPR40* mRNA in human pancreas and isolated islets

The expression of *GPR40* mRNA in human tissues was assessed by TaqMan PCR using total RNA samples from patients who underwent pancreatectomy and/or other pertinent surgeries. *GPR40* mRNA was detected in all human pancreases examined (n=12), and at higher levels than those in the duodenum, jejunum or liver (Fig. 1a). The inter-individual variability in the *GPR40* mRNA levels was considerable in the human pancreas. The *GPR40* mRNA level in the pancreas was not significantly different between sites (head vs body) of the pancreas or between men and women. The *GPR40* mRNA level in the pancreas did not correlate significantly with age. The *GPR40* mRNA level in fresh islets that were isolated from pancreatic tissues (n=3) was approximately 20-fold higher than that in the pancreas from the same patients (Fig. 1b).

To gain further insight into the expression of the *GPR40* gene in pancreatic islets, we analysed the expression of genes known to be expressed abundantly in the pancreatic islets. The estimated mRNA copy number of the *GPR40* gene in isolated islets was comparable to or higher than those of genes encoding receptors for sulfonylurea, glucagon-like peptide 1 and somatostatin (Fig. 1c), suggesting that high levels of the *GPR40* gene are expressed in pancreatic islets.

Expression of *GPR40* mRNA in insulinoma tissues

We analysed the expression of *GPR40* mRNA in islet cell tumours, including insulinoma (n=3), glucagonoma (n=1)

Table 2 Sequences of TaqMan primers and probes

Gene	Forward primer (5′→3′)	Probe (FAM-5′→3′-TAMRA)	Reverse Primer (5′→3′)	Accession number
GPR40	GCCCGCTTCAGCC TCTCT	TCTGCCCTTGGCCATCA CAGCCT	GAGGCAGCCCAC GTAGCA	NM_005303
GLP1R	GCAGCCCTGAAGTGG ATGTATAG	ACAGCCGCCCAGCAGCA CCAGT	CTCAGAGAGTCCT GGTAGGAGAG	NM_002062
ABCC8	GCTGCCCATCGTTATG AGGG	CCTCACCAACTACCAACG GCTCTGCG	GAATGTCCTTCCG CACCTGG	NM_000352
SSTR3	CCGTCAGTGGCGTTCT GATCC	CCACCACGCACACCACC AGGTAGACC	ATAGATGACCAGC GAGTTACCCAG	NM_001051
SSTR5	CTCGGAGCGGAAGGT GACG	AACACCAGCACCACCACCAA CACCAT	GTGAAGAAGGGCA GCCAACATC	NM_001053
GAPDH	TGAAGCAGGCGTCGG AGG	CCTCAAGGGCATCCTGGGCTA CACTG	GCTGTTGAAGTCAG AGGAGACC	NM_002046

The *ABCC8* gene is also known as *SUR1* and encodes sulfonylurea receptor 1
FAM 6-carboxyfluorescein, *TAMRA* 6-carboxytetramethylrhodamine

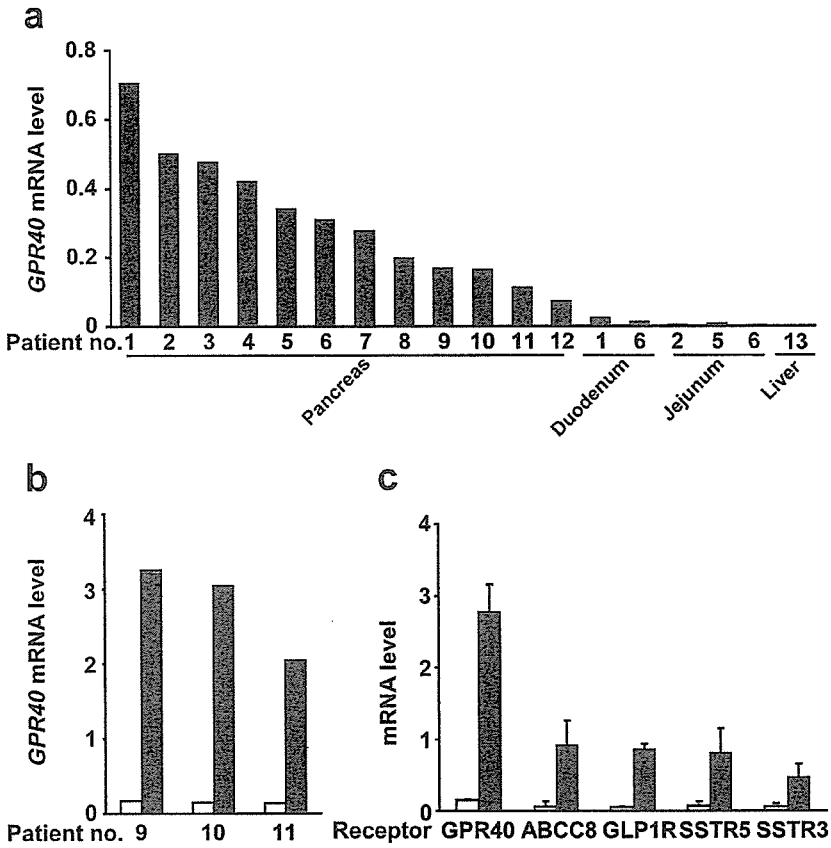

Fig. 1 TaqMan quantitative analyses of *GPR40* mRNA expression in human pancreatic tissues. Total RNA extracted from various tissues was analysed. **a** *GPR40* mRNA was detected in all human pancreas specimens examined, at higher abundance than in the duodenum, jejunum or liver. Patients 1–12 were numbered according to their relative level of expression of *GPR40* mRNA. **b** *GPR40* mRNA level in isolated islets was ~20-fold higher than in pancreatic tissues from the same patients. The numbers in **a** and **b** correspond to those in Table 1. **c** Estimated mRNA copy number of the *GPR40* gene was similar to or higher than those for genes encoding sulfonylurea receptor 1 (*ABCC8*), glucagon-like peptide 1 receptor (*GLP1R*) and somatostatin receptors 3 (*SSTR3*) and 5 (*SSTR5*) (n=3). Data are means±SEM. *Open bars* pancreas; *closed bars* isolated islets

and gastrinoma (n=1). *GPR40* mRNA was detected in tissue extracts from three cases of insulinoma (Fig. 2), which was comparable to that in pancreatic islets (Fig. 2). *GPR40* mRNA was below detectable levels in tissue extracts from glucagonoma or gastrinoma (Fig. 2).

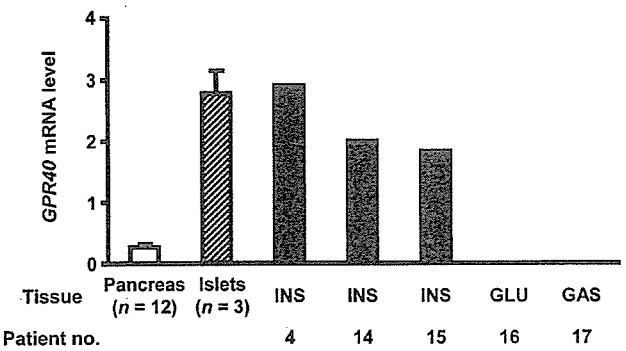

Fig. 2 TaqMan quantitative analyses of *GPR40* mRNA expression in human islet cell tumours. Total RNA extracted from pancreases (n=12), pancreatic islets (n=3) and islet cell tumours (patients 4, 14, 15, 16, 17) was analysed. *GPR40* mRNA was abundantly expressed in three cases of insulinoma among islet cell tumours. *Open bar*, pancreas; *hatched bar*, pancreatic islets; *closed bars*, islet cell tumours. The patient numbers in the figure correspond to those in Table 1. The *GPR40* mRNA level in the pancreas and pancreatic islets is expressed as mean±SEM. *INS* insulinoma, *GLU* glucagonoma, *GAS* gastrinoma

The correlation between the *GPR40* mRNA level in the pancreas and insulinogenic index is positive

To understand the physiological role of GPR40 in humans, we examined the relationship between the *GPR40* mRNA level in the pancreas and various metabolic parameters. Table 3 summarises the metabolic profiles of patients who underwent pancreatectomy. The *GPR40* mRNA level in the pancreas did not correlate significantly with BMI, fasting plasma glucose, plasma glucose at 2 h under the OGTT (2h-PG) or insulin AUC. Furthermore, the *GPR40* mRNA level in the pancreas did not correlate significantly with the HOMA-IR (n=10) (Fig. 3a). The significant positive correlation between the *GPR40* mRNA level in the pancreas and the insulinogenic index was notable (n=7) (p=0.044, r=0.82) (Fig. 3b). To verify the significant association, correlation was tested between the *GPR40* mRNA level in the pancreas and the HOMA-IR, using data from the same patients from whom data on the insulinogenic index were available (n=7), and we confirmed that there was no significant correlation between the *GPR40* mRNA level and the HOMA-IR (p=0.86, r=0.07). The *GPR40* mRNA level in the pancreas was not significantly associated with HbA_{1c} or fasting triglyceride.

Table 3 Metabolic profiles of patients studied

Patient	BMI (kg/m^2)	FPG (mmol/l)	2h-PG (mmol/l)	Insulin AUC ($\times 10^3$ pmol/l)	HOMA-IR	Insulinogenic index	HbA_{1c} (%)	Triglycerides (mmol/l)
1	17.7	4.4	6.8	41.8	2.8	62.7	4.7	1.54
2	19.7	7.2	12.6	102.2	36.6	100.1	6.7	2.26
3	23.5	4.9	8.9	280.8	10.3	ND	5.8	1.99
4[a]	22.1	2	4.9	ND	2.5	ND	4.3	0.86
5	18.4	6.1	ND	ND	ND	ND	6.1	2.03
6	22.6	5.4	8.3	103.0	6.8	47.8	5.8	1.60
7	21.6	5.7	8.5	82.8	11.6	51.0	5.5	1.60
8	22.8	5.5	13.6	78.5	8.5	ND	6.3	2.28
9	18	5.3	10.8	22.2	3.3	23.6	5.9	1.76
10	23	4.9	ND	ND	ND	ND	5.1	1.33
11	22.3	4.9	9.1	36.0	3.7	17.8	5.3	0.89
12	24.6	5.1	8.3	44.9	5.7	42.8	4.7	1.20

[a]Patient 4 was diagnosed as having insulinoma
Because of the unavailability of blood samples, some of the metabolic profiles were not determined (shown as ND)
2h-PG Plasma glucose at 2 h under the OGTT, *FPG* fasting plasma glucose, *ND* not determined

Discussion

GPR40 is abundantly expressed in murine pancreatic beta cells [3, 7] where it mediates the fatty acid-induced augmentation of GSIS in vitro [6]. Long-chain fatty acids act as ligands for human GPR40 in vitro [3, 7, 23]. Additionally, two studies suggest the possible involvement of GPR40 in the proliferation and cell function of breast cancer [27, 28]. Two laboratories reported the possible relationship between variation of the *GPR40* single-nucleotide polymorphisms and insulin secretion in humans [22, 23], where the results were inconsistent. The physiological role of GPR40 in humans remains obscure.

We here demonstrate for the first time that a large amount of *GPR40* mRNA is expressed in pancreatic islets in humans using expeditiously isolated islets from pancreatic tissue. TaqMan analysis revealed that levels of *GPR40* mRNA expression in pancreatic islets were 20-fold higher than those in the pancreas in the same individuals. Notably, the mRNA level of the *GPR40* gene in isolated islets was comparable to those of genes encoding GLP1R, ABCC8 (SUR1) and SSTRs, all of which are abundantly expressed in human pancreatic islets [13–16].

The present study demonstrates that a large amount of *GPR40* mRNA is expressed solely in three cases of insulinoma among islet cell tumours. The finding suggests that the *GPR40* mRNA detected in insulinoma is attributed to the type of islet cell tumour rather than the inclusion of endothelial, neuronal or other types of cells. Collectively, these data prompt us to speculate that GPR40 is expressed mainly in beta cells in the human pancreatic islet.

It is noteworthy that the mRNA levels of *GPR40* and *ABCC8* (*SUR1*) were comparable in human pancreatic islets, because *ABCC8* (*SUR1*) is abundantly expressed in

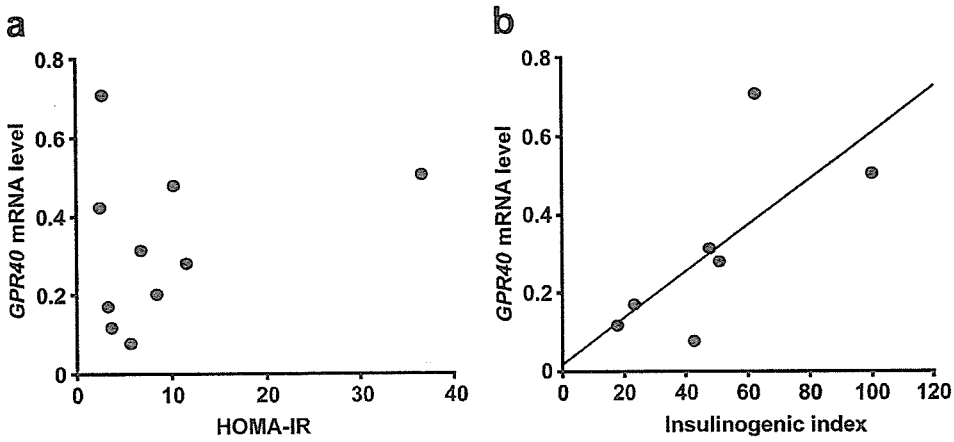

Fig. 3 Positive correlation between *GPR40* mRNA level in the pancreas and insulinogenic index. **a** Relationship between *GPR40* mRNA level in the pancreas and the HOMA-IR (n=10). *GPR40* mRNA level and the HOMA-IR did not correlate significantly (r=0.11, p=0.73). **b** Relationship between *GPR40* mRNA level in the pancreas and the insulinogenic index (n=7). Correlation was marginally but significantly positive between *GPR40* mRNA level and the insulinogenic index (r=0.82, p=0.044). Spearman's rank correlation test was used to determine p and r values. The solid line is the regression line

human pancreatic beta cells and the protein functions as a target of sulfonylurea agents [29]. These findings suggest that GPR40 has also some functional property in terms of insulin secretion in humans. In the present study, the *GPR40* mRNA level in the pancreas significantly correlated with the insulinogenic index rather than the HOMA-IR, supporting the notion that GPR40 is involved in the regulation of insulin secretion in humans.

A recent study of *GPR40* knockout mice and beta-cell-specific *GPR40* transgenic mice provided evidence that GPR40 is involved in the pathophysiology of glucose intolerance and beta cell lipotoxicity [11]. In this context, it is important to note that patients enrolled in the present study were neither obese nor severely diabetic. Thus, clarification of the pathophysiological role of GPR40 in human diabetes must await further investigation in patients with a wider range of body weight, glucose intolerance or dyslipidaemia.

As pancreatic tissues are very vulnerable to postmortem autolysis, specimens obtained at operation have a great advantage for the precise analysis of the *GPR40* mRNA level. Pancreatic biopsy is rarely conducted because of the risk of pancreatitis and is not justified in those without severe illness [30]. Thus, we analysed human pancreatic tissues collected during surgery. To our knowledge, specific antibody against human GPR40 has not been available, hence the lack of analyses of GPR40 protein expression in the present study.

In summary, the present study demonstrates that *GPR40* mRNA is abundantly expressed in human pancreatic islets and insulinoma. The results provide evidence for GPR40 expression in pancreatic beta cells and its involvement in insulin secretion in humans.

Acknowledgements We are grateful to M. Nagamoto for excellent technical assistance. This study was supported in part by a research grant from Special Coordination Funds for Promoting Science and Technology (JST, Japan); a Grant-in-Aid for Scientific Research (S2) (16109007), a Grant-in-Aid for Scientific Research (B2) (16390267), a Grant-in-Aid for Exploratory Research (16659243), and a Grant-in-Aid for Scientific Research on Priority Areas (15081101) from the Japanese Ministry of Education, Culture, Sports, Science and Technology; a Grant-in-Aid for Research (Japanese Ministry of Health, Labor and Welfare); a research award from the Japan Foundation for Applied Enzymology; the Yamaguchi Endocrine Research Association; the Cell Science Research Foundation; the Takeda Medical Research Foundation; the Smoking Research Foundation; and the Metabolic Syndrome Research Foundation. The authors are not aware of any duality of interest.

References

1. Nunez EA (1997) Biological complexity is under the 'strange attraction' of non-esterified fatty acids. Prostaglandins Leukot Essent Fat Acids 57:107–110
2. Corkey BE, Deeney JT, Yaney GC, Tornheim K, Prentki M (2000) The role of long-chain fatty acyl-CoA esters in beta-cell signal transduction. J Nutr 130:299S–304S
3. Briscoe CP, Tadayyon M, Andrews JL et al (2003) The orphan G protein-coupled receptor GPR40 is activated by medium and long chain fatty acids. J Biol Chem 278:11303–11311
4. McGarry JD, Dobbins RL (1999) Fatty acids, lipotoxicity and insulin secretion. Diabetologia 42:128–138
5. Unger RH (2003) Minireview: weapons of lean body mass destruction: the role of ectopic lipids in the metabolic syndrome. Endocrinology 144:5159–5165
6. Itoh Y, Kawamata Y, Harada M et al (2003) Free fatty acids regulate insulin secretion from pancreatic beta cells through GPR40. Nature 422:173–176
7. Kotarsky K, Nilsson NE, Flodgren E, Owman C, Olde B (2003) A human cell surface receptor activated by free fatty acids and thiazolidinedione drugs. Biochem Biophys Res Commun 301:406–410
8. Brown AJ, Goldsworthy SM, Barnes AA et al (2003) The orphan G protein-coupled receptors GPR41 and GPR43 are activated by propionate and other short chain carboxylic acids. J Biol Chem 278:11312–11319
9. Nilsson NE, Kotarsky K, Owman C, Olde B (2003) Identification of a free fatty acid receptor, FFA2R, expressed on leukocytes and activated by short-chain fatty acids. Biochem Biophys Res Commun 303:1047–1052
10. Hirasawa A, Tsumaya K, Awaji T et al (2005) Free fatty acids regulate gut incretin glucagon-like peptide-1 secretion through GPR120. Nat Med 11:90–94
11. Steneberg P, Rubins N, Bartoov-Shifman R, Walker MD, Edlund H (2005) The FFA receptor GPR40 links hyperinsulinemia, hepatic steatosis, and impaired glucose homeostasis in mouse. Cell Metabolism 1:245–258
12. Cameron, JL, Mehigan DG, Harrington DP, Zuidema GD (1980) Metabolic studies following intrahepatic autotransplantation of pancreatic islet grafts. Surgery 87:397–400
13. Giannaccini G, Lupi R, Trincavelli ML et al (1998) Characterization of sulfonylurea receptors in isolated human pancreatic islets. J Cell Biochem 71:182–188
14. Dillon JS, Tanizawa Y, Wheeler MB et al (1993) Cloning and functional expression of the human glucagon-like peptide-1 (GLP-1) receptor. Endocrinology 133:1907–1910
15. Thorens B, Porret A, Buhler L, Deng SP, Morel P, Widmann C (1993) Cloning and functional expression of the human islet GLP-1 receptor. Demonstration that exendin-4 is an agonist and exendin-(9–39) an antagonist of the receptor. Diabetes 42:1678–1682
16. Kumar U, Sasi R, Suresh S et al (1999) Subtype-selective expression of the five somatostatin receptors (hSSTR1-5) in human pancreatic islet cells: a quantitative double-label immunohistochemical analysis. Diabetes 48:77–85
17. Iwakura H, Hosoda K, Son C et al (2005) Analysis of rat insulin II promoter-ghrelin transgenic mice and rat glucagon promoter-ghrelin transgenic mice. J Biol Chem 280: 15247–15256
18. Iwakura H, Hosoda K, Doi R et al (2002) Ghrelin expression in islet cell tumors: augmented expression of ghrelin in a case of glucagonoma with multiple endocrine neoplasm type I. J Clin Endocrinol Metab 87:4885–4888
19. Li Y, Kishimoto I, Saito Y et al (2004) Androgen contributes to gender-related cardiac hypertrophy and fibrosis in mice lacking the gene encoding guanylyl cyclase-A. Endocrinology 145:951–958
20. Saito S, Iida A, Sekine A et al (2002) Identification of 779 genetic variations in eight genes encoding members of the ATP-binding cassette, subfamily C (ABCC/MRP/CFTR). J Hum Genet 47:147–171
21. Haga H, Yamada R, Ohnishi Y, Nakamura Y, Tanaka T (2002) Gene-based SNP discovery as part of the Japanese Millennium Genome Project: identification of 190,562 genetic variations in the human genome. Single-nucleotide polymorphism. J Hum Genet 47:605–610
22. Ogawa T, Hirose H, Miyashita K, Saito I, Saruta T (2005) GPR40 gene Arg211His polymorphism may contribute to the variation of insulin secretory capacity in Japanese men. Metabolism 54:296–299

23. Hamid YH, Vissing H, Holst B et al (2005) Studies of relationships between variation of the human G protein-coupled receptor 40 gene and type 2 diabetes and insulin release. Diabet Med 22:74–80
24. Ferrannini E, Gastaldelli A, Miyazaki Y, Matsuda M, Mari A, DeFronzo RA (2005) Beta-cell function in subjects spanning the range from normal glucose tolerance to overt diabetes: a new analysis. J Clin Endocrinol Metab 90:493–500
25. Matthews DR, Hosker JP, Rudenski AS, Naylor BA, Treacher DF, Turner RC (1985) Homeostasis model assessment: insulin resistance and beta-cell function from fasting plasma glucose and insulin concentrations in man. Diabetologia 28:412–419
26. Takahashi-Yasuno A, Masuzaki H, Miyawaki T et al (2004) Association of Ob-R gene polymorphism and insulin resistance in Japanese men. Metabolism 53:650–654
27. Yonezawa T, Katoh K, Obara Y (2004) Existence of GPR40 functioning in a human breast cancer cell line, MCF-7. Biochem Biophys Res Commun 314:805–809
28. Hardy S, St-Onge GG, Joly E, Langelier Y, Prentki M (2005) Oleate promotes the proliferation of breast cancer cells via the G protein-coupled receptor GPR40. J Biol Chem 280: 13285–13291
29. Gribble FM, Reimann F (2003) Sulphonylurea action revisited: the post-cloning era. Diabetologia 46:875–891
30. Imagawa A, Hanafusa T, Uchigata Y et al (2005) Different contribution of class II HLA in fulminant and typical autoimmune type 1 diabetes mellitus. Diabetologia 48:294–300

Notch/Rbp-j signaling prevents premature endocrine and ductal cell differentiation in the pancreas

Junji Fujikura,[1] Kiminori Hosoda,[1,*] Hiroshi Iwakura,[1] Tsutomu Tomita,[1] Michio Noguchi,[1] Hiroaki Masuzaki,[1] Kenji Tanigaki,[2] Daisuke Yabe,[2] Tasuku Honjo,[2] and Kazuwa Nakao[1]

[1] Department of Medicine and Clinical Science, Kyoto University Graduate School of Medicine, 54 Shogoin-Kawahara-cho, Sakyo-ku, Kyoto 606-8507, Japan
[2] Department of Medical Chemistry, Kyoto University Graduate School of Medicine, Yoshida-Konoe-cho, Sakyo-ku, Kyoto 606-8501, Japan
*Correspondence: pekopaokuro@yahoo.co.jp

Summary

To investigate the precise role of Notch/Rbp-j signaling in the pancreas, we inactivated Rbp-j by crossing Rbp-j floxed mice with *Pdx.cre* or *Rip.cre* transgenic mice. The loss of Rbp-j at the initial stage of pancreatic development induced accelerated α and PP cell differentiation and a concomitant decrease in the number of Neurogenin3 (Ngn3)-positive cells at E11.5. Then at E15, elongated tubular structures expressing ductal cell markers were evident; however, differentiation of acinar and all types of endocrine cells were reduced. During later embryonic stages, compensatory acinar cell differentiation was observed. The resultant mice exhibited insulin-deficient diabetes with both endocrine and exocrine pancreatic hypoplasia. In contrast, the loss of Rbp-j specifically in β cells did not affect β cell number and function. Thus, our analyses indicate that Notch/Rbp-j signaling prevents premature differentiation of pancreatic progenitor cells into endocrine and ductal cells during early development of the pancreas.

Introduction

The pancreas plays a key role in the maintenance of nutritional homeostasis through its exocrine and endocrine functions. The acini and ducts form the exocrine pancreas that produces and transports digestive enzymes into the duodenum. Besides, there are five known endocrine cell types in the pancreas: glucagon-producing α cells, insulin-producing β cells, somatostatin-producing δ cells, pancreatic polypeptide (PP)-producing PP cells, and ghrelin-producing ε cells (Heller et al., 2005).

Notch signaling regulates various developmental processes, such as neurogenesis, somitogenesis, angiogenesis, and hematopoiesis (Ishibashi et al., 1995; Hrabé de Angelis et al., 1997; Xue et al., 1999; Han et al., 2002). Interaction of a Notch receptor with its ligand induces cleavage of the receptor's intracellular domain (Notch ICD), which translocates to the nucleus and binds to Rbp-j to induce the expression of Hes family transcriptional repressors (Kageyama and Ohtsuka, 1999). Rbp-j is a key mediator of Notch signaling because it is expressed ubiquitously and associates with all four types of Notch receptors (Kato et al., 1996). Various Notch-related genes are expressed in the developing pancreas (Lammert et al., 2000). However, multiple anomalies and early embryonic lethalities of mice with homozygous deletions of genes such as *Dll1*, *Notch1*, *Notch2*, *Jagged1*, *Rbp-j*, or *Hes1* limits assessment of the importance of Notch/Rbp-j signaling in the pancreas (Swiatek et al., 1994; Ishibashi et al., 1995; Oka et al., 1995; Hrabé de Angelis et al., 1997; Apelqvist et al., 1999; Hamada et al., 1999; Xue et al., 1999; Jensen et al., 2000a). Although excess α cell differentiation in the pancreas has been reported at around E10 in mice with a generalized KO of Dll1 or Hes1 (Apelqvist et al., 1999; Jensen et al., 2000a), because β cells start to expand at around E13 and their differentiation occurs independently of α cells (Jensen et al., 2000b), the influence of Notch signaling on β cells remains to be elucidated. To address this issue, we created mice with developmental stage-specific deletion of *Rbp-j* in the pancreas using the Cre/loxP-mediated DNA recombination system.

Results

Accelerated premature differentiation of α and PP cells but not of β, δ, and ε cells in pancreatic Rbp-j KO (PRKO) mice

By crossing floxed Rbp-j (*Rbp-j*$^{f/f}$, designated as F/F) mice with *Pdx.cre* mice, we generated pancreatic Rbp-j KO (*Rbp-j*$^{f/f}$ *Pdx.cre*, designated as PRKO) mice (Gu et al., 2002; Han et al., 2002; see the Supplemental Data available with this article online). The *Pdx.cre* mouse begins to recombine loxP sites in the pancreatic epithelium before E9.5 (Figure S1B). Notch signaling negatively regulates proneural basic helix-loop-helix (bHLH) factors through Hes activation (Kageyama and Ohtsuka, 1999). A unique proendocrine bHLH transcription factor, Ngn3, is required for the development of pancreatic endocrine lineages (Gradwohl et al., 2000; Gu et al., 2002). We observed a premature increase in the number of Ngn3$^+$ cells in the pancreatic buds of PRKO mice (Figure S2A). At E11.5, a few scattered α cells among the protruding epithelial cells of F/F mice were observed (Figures 1E and 1E′). In PRKO mice, the number of α and PP cells increased and they surrounded the pancreatic buds (Figures 1F, 1F′, 1J, and 1J′). However, β, δ, and ghrelin-producing cell differentiation was not enhanced in the mutants (Figures 1D, 1D′, 1H, 1H′, and S3B). The number of Ngn3$^+$ cells decreased in PRKO mice compared with control mice (Figures 1M–1N′ and S2B). The number of proliferating cells detected by phosphohistone H3 (pHH3) immunostaining was comparable between control and mutant mice (Figures 1O–1P′). No apoptotic cells were

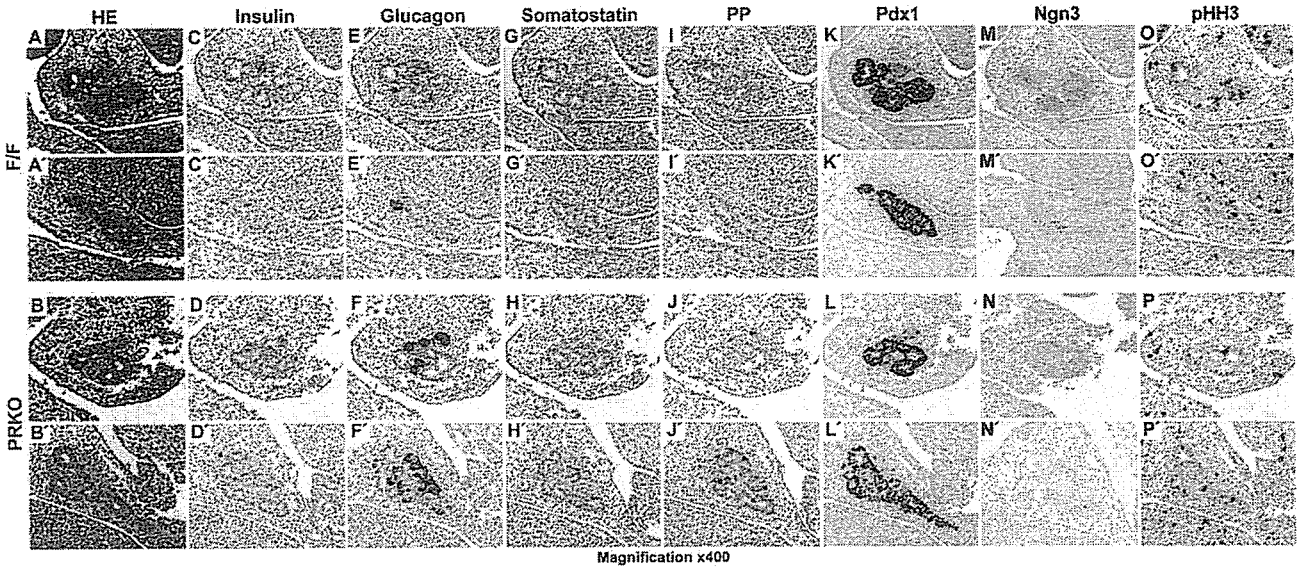

Figure 1. Accelerated premature differentiation of α and PP cells but not β, δ, and ε cells in pancreatic Rbp-j KO (PRKO) mice

A–P′) HE staining (**A–B′**), and immunostaining (**C–P′**) of representative serial pancreatic sections from F/F mice and PRKO mice at E11.5.

detected in the pancreatic epithelia of control or mutant mice (Figures S3C–S3E). These data indicate that earlier commitment to proendocrine ($Ngn3^+$) cells induced by defective Notch signaling results in precocious endocrine cell differentiation and a substantial loss of proendocrine cells during early pancreatic development.

Elongated tubular structures with decreased branching morphogenesis in the pancreas of the PRKO mouse

At E15, pancreatic $Pdx1^+$ epithelium of control mice exhibited complex and ramified networks (Figure 2B). However, in the mutant, branching of $Pdx1^+$ epithelium was severely impaired, and dilated tubular structures were prominent (Figure 2B′). The decreased epithelial branching was not associated with increased cell death or decreased proliferation, because these cells were not apoptotic (Figure 2D′), but exhibited active division (Figure 2M′). Moreover, acinar and β cells were scarcely differentiated (Figures 2C′ and 2H′), and aggregated α cells existed around the columnar tubular epithelium (Figure 2G′). The cells lining the lumens of tubular structures showed positive staining with cytokeratin (CK) and Dolichos biflorus agglutinin (DBA) lectin (Dor et al., 2004) (Figures 2K–2L′). The glucose transporter 2 (Glut2), expressed on the surface of differentiated β cells (Figure 2N), is also thought to be a marker of early pancreatic progenitor cells (Pang et al., 1994); however, Glut2 was not expressed in the tubular epithelium (Figure 2N′). In the control pancreas, *Hes1* expression was not detected (Figure 2O), but scattered $Ngn3^+$ cells were evident at this stage (Figure 2P). In the mutant pancreas, expression of *Hes1* and Ngn3 was virtually absent (Figures 2O′ and 2P′). ISL1 is a LIM homeodomain protein whose expression is initiated after Ngn3 extinction but before hormone production (Ahlgren et al., 1997). ISL1 expression was not detected in the tubular epithelium (Figure 2Q′). This analysis of various differentiation markers shows that the cells lining these tubular structures are not early progenitors, nor are they on the endocrine lineage. The tubular morphologies and high columnar epithelium resembling that of the large pancreatic duct rather suggest that the cells positive for ductal markers are duct cells. We confirmed that all of these cells were derived from Rbp-j-deficient cells by lineage tracing (Figure S4).

At later embryonic stages of PRKO mice, the acinar cell area was much smaller and CK^+ ductal cells occupied a larger area compared with F/F mice (Figures S5A–S5F). Although compensatory acinar growth was observed (Figures S5E–S5H), the interval sections revealed a much smaller pancreas in the mutant than in the control mouse (Figure S5I).

PRKO mice are born with pancreatic hypoplasia and exhibit insulin-deficient diabetes

The adult PRKO mouse exhibited a small pancreas (Figure 3A). The absolute pancreatic weight (PRKO, 209 ± 73 mg versus F/F, 685 ± 81 mg; $p = 0.0038$; Figure 3B) and the ratio of pancreatic weight to total body weight (data not shown) were lower in PRKO mice than in F/F mice. In pancreatic sections from PRKO mice, the number of islets per pancreas area was reduced (PRKO, 0.15 ± 0.06 versus F/F, 0.62 ± 0.13 islets/mm^2; $p = 0.015$; Figures 3C and 3D), and the size of the islets was smaller compared with F/F mice (Figure 3C). The relative endocrine cell mass was quantified by estimating the hormone-positive area per total pancreatic area in multiple pancreatic sections. The β cell mass of the PRKO mice was markedly reduced to about 25% of the β cell mass of F/F mice (PRKO, 0.21 ± 0.08% versus F/F, 1.13 ± 0.04%; $p < 0.001$; Figure 3E), and the absolute α cell mass was also significantly reduced to about 50% of that of the F/F mice (PRKO, 0.11 ± 0.02% versus F/F, 0.24 ± 0.02%; $p < 0.001$; Figure 3E). Total pancreatic insulin content (expressed per mg of pancreas weight) estimated from an acid-ethanol extract of the whole pancreas. PRKO mice had much lower insulin contents

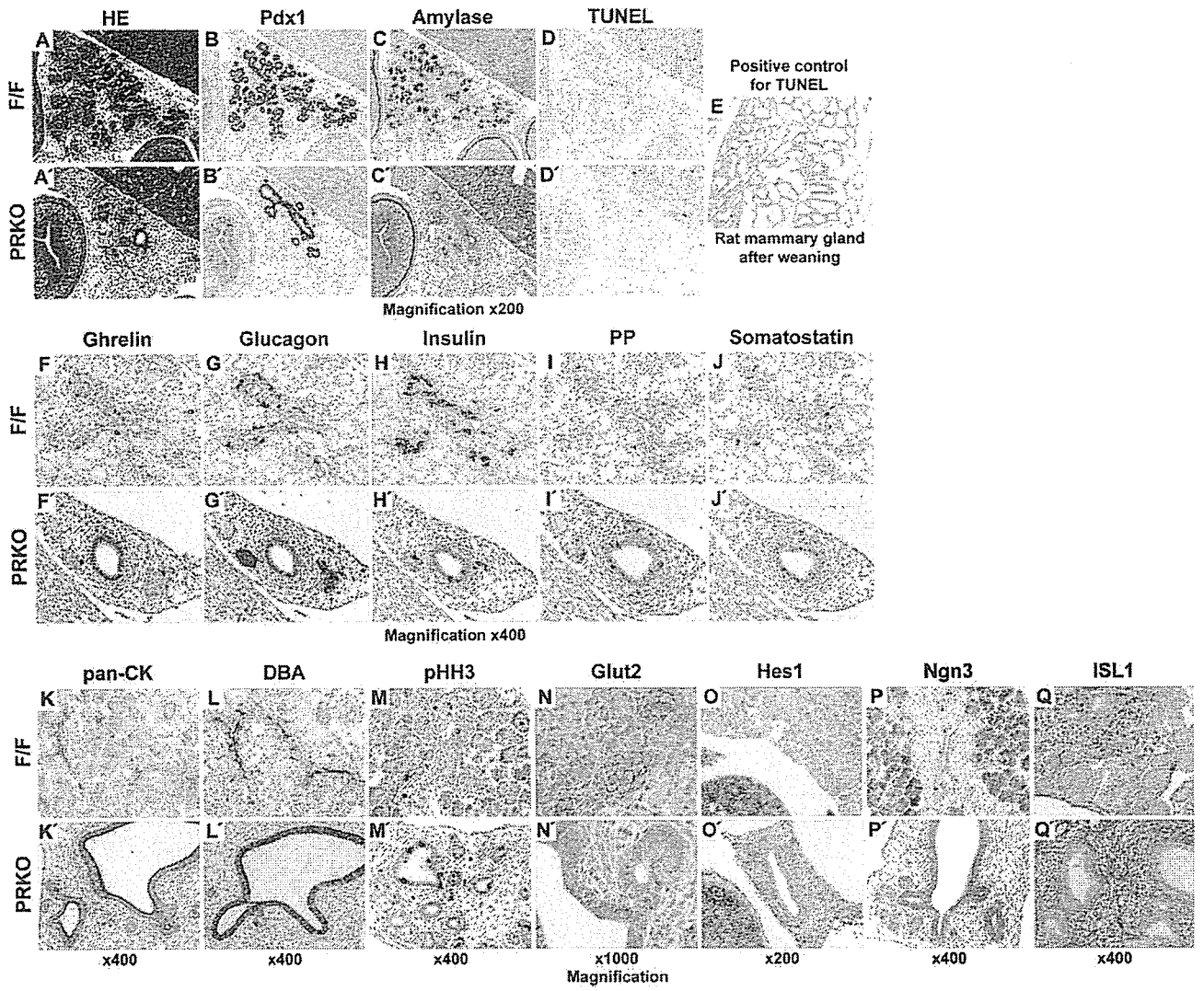

Figure 2. Elongated tubular structures with decreased branching in PRKO mice at E15

A–J′) Dilated and elongated duct-like structures in PRKO mice. HE staining (**A and A′**), immunostaining (**B–C′ and F–J′**), and TUNEL assay (**D and D′**) of serial pancreatic sections from F/F mice and PRKO mice at E15. The mammary gland of a postlactating female Wistar rat was used as a positive control for apoptosis (**E**).

K–Q′) Characterization of duct-like cells in PRKO mice. Immunostaining (**K–N′, P–Q′**) and *Hes1* in situ hybridization (**O and O′**) of pancreatic sections from F/F and PRKO mice at E15.

than the F/F mice (PRKO, 0.9 ± 0.2 pg/mg pancreas versus F/F, 96.4 ± 9.9 pg/mg pancreas; $p < 0.001$; Figure 3F). In addition to the scarcity of islets, histological analysis of the adult pancreas in PRKO mice revealed that the endocrine cells were frequently observed in association with distended pancreatic ducts (Figures 3J, 3L, 3N, 3P, and 3R). The relative ductal hyperplasia observed during the embryonic stages of PRKO mice (Figure S5D) became obscured in adult PRKO mice (Figure 3C).

The growth of PRKO mice and F/F mice fed normal chow was observed for four months. PRKO mice had a leaner phenotype than F/F mice and exhibited no further weight gain (Figures 3S and 3T). At eight weeks of age, PRKO mice developed significant hyperglycemia during fasting and feeding (fasting—PRKO, 348 ± 61 mg/dl versus F/F, 98 ± 6 mg/dl; $p < 0.001$; morning fed—PRKO, 524 ± 59 mg/dl versus F/F, 124 ± 12 mg/dl; $p < 0.001$; Figure 3U), which was accompanied by notably decreased plasma insulin concentrations (fasting—PRKO, below detection limit versus F/F, 0.48 ± 0.07 ng/ml; $p < 0.001$; morning fed—PRKO 0.04 ± 0.03 ng/ml versus F/F, 1.35 ± 0.25 ng/ml; $p = 0.0013$; Figure 3V). At this age, the mutant mice showed polyuria and polydipsia, and some appeared lethargic. Daily food intake increased in PRKO mice compared with control mice (PRKO, 8.3 ± 0.6 g/24 hr versus F/F, 4.1 ± 0.3 g/24 hr; $p < 0.001$; Figure 3W), which corresponded to diabetic hyperphagia. Thus, PRKO mice exhibited characteristics typical of diabetes with defective insulin secretion. Furthermore, PRKO mice had lower serum amylase activities than F/F mice (PRKO, 711 ± 58 U/dl versus F/F, 1121 ± 67 U/dl; $p = 0.0015$; Figure 3X), presumably due to pancreatic hypoplasia and severe diabetes.

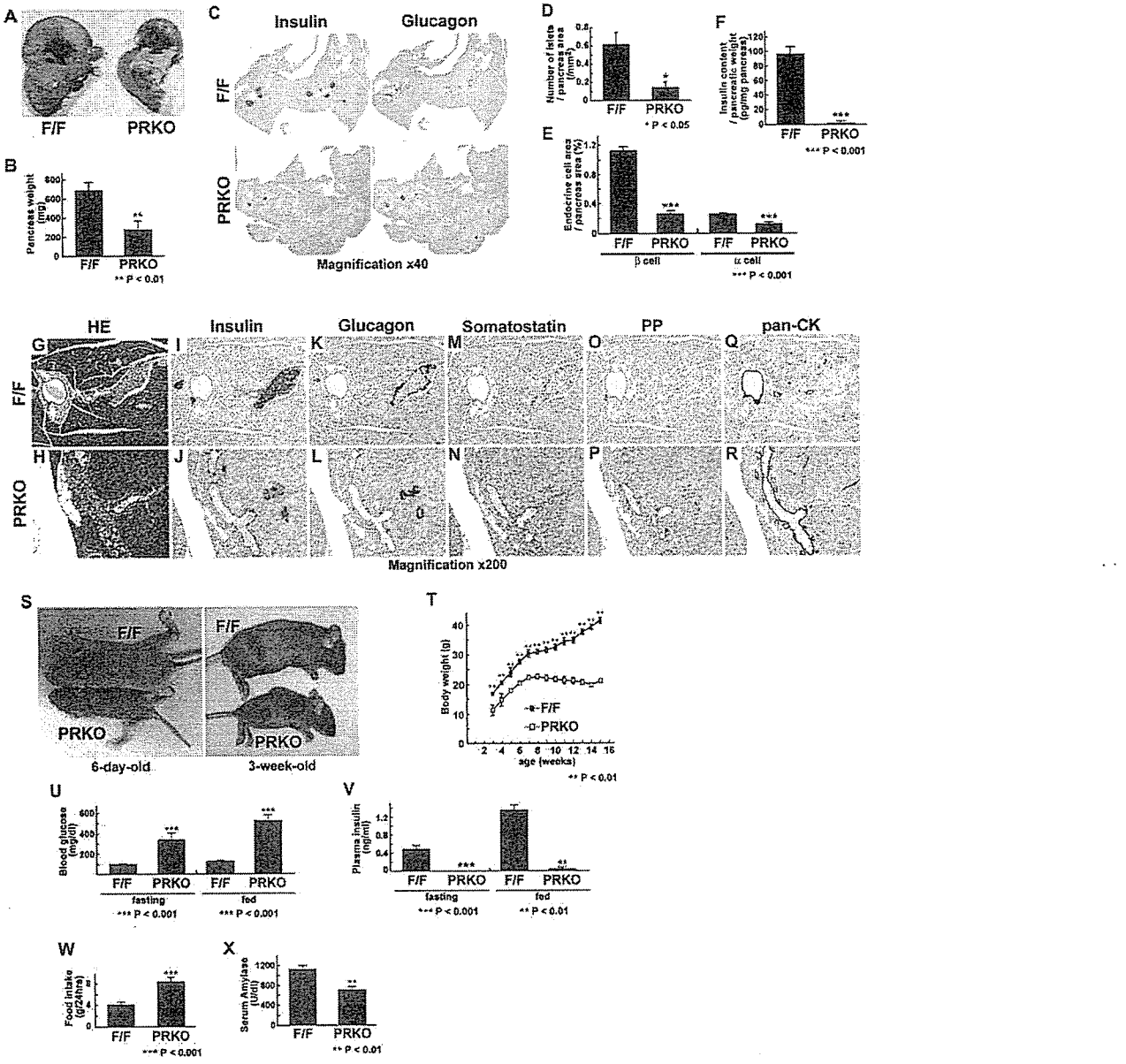

Figure 3. The adult PRKO mouse has a small pancreas, few islets, and low insulin content, which result in overt diabetes

A and B) Small pancreas in an adult PRKO mouse. Gut regions were dissected **(A)**, and pancreatic weights were measured at 12 weeks of age **(B)**.

C–E) Fewer islets and reduced endocrine cell mass in PRKO mice. Pancreatic sections from 10-week-old F/F mice and PRKO mice were immunostained for insulin and glucagon **(C)** to determine the number of islets **(D)**, β cell area **(E)**, and α cell area **(E)**, which were normalized to total pancreatic area.

F) Lower pancreatic insulin content in PRKO mice. Pancreatic insulin content was measured in acid-ethanol extracts from 6-week-old F/F mice and PRKO mice.

G–R) Duct-associated endocrine cells in PRKO mice. HE staining **(G and H)** and immunostaining **(I–R)** of serial pancreatic sections from 8-week-old F/F and PRKO mice. The number of β cells was markedly reduced **(J)**. Endocrine cells are located close to ductal structures **(J, L, N, and P)**.

S and T) Growth retardation in PRKO mice. Gross appearances **(S)** of 6-day-old (left) and 3-week-old (right) PRKO mice (bottom) and control littermates (top). Growth curve **(T)** for litters obtained from mating F/F mice and PRKO mice.

U–W) Insulin-deficient diabetes in PRKO mice. Blood glucose concentrations **(U)** and plasma insulin concentrations **(V)** from fasted and random-fed 8-week-old male F/F mice and PRKO mice. Food intake **(W)** was measured for 24 hr from 16-week-old male F/F mice and PRKO mice.

X) Exocrine pancreatic insufficiency in F/F *Rip.cre* mice. Amylase activity was measured in serum from F/F mice and PRKO mice at 10 weeks of age.

Bars represent means ± SE of n = 4–8 mice. Levels of significance (Student's t test) are shown (*p < 0.05; **p < 0.01; ***p< 0.001).

β cell-specific Rbp-j KO (βRKO) mice have normal β cell number and function

By crossing F/F mice with *Rip.cre* mice, we next generated β cell-specific Rbp-j KO (*Rbp-j*$^{f/f}$ *Rip.cre*, designated as βRKO) mice (Figure S6). βRKO mice had normal body weight (βRKO, 35.2 ± 2.6 mg/dl versus *Rip.cre*, 37.0 ± 2.5 mg/dl; p = 0.62; Figure 4A). No significant differences were detected in the levels of blood glucose (βRKO, 160 ± 17 mg/dl versus *Rip.cre*,

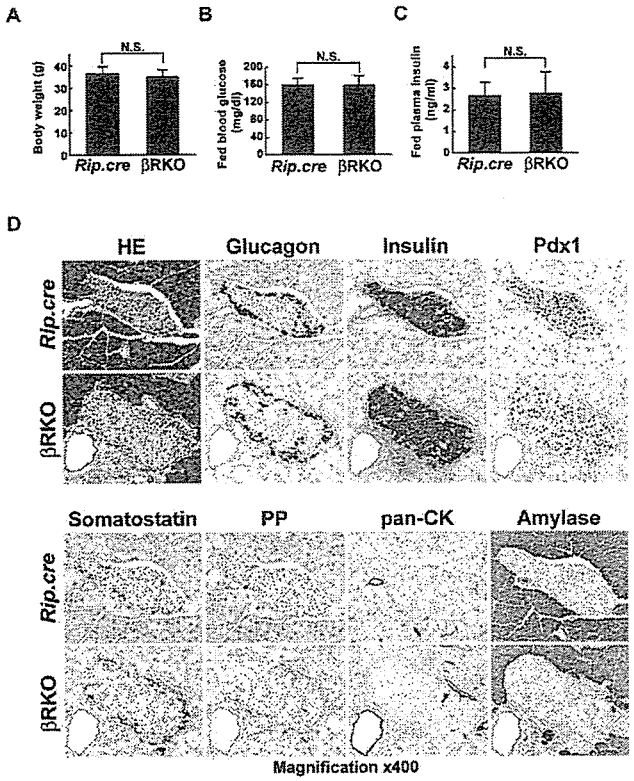

Figure 4. Absence of abnormalities in β cell-specific *Rbp-j* KO mice

A–C) Metabolic parameters of βRKO mice. Body weight **(B)**, random-fed blood glucose concentrations **(C)**, and random-fed plasma insulin concentrations **(D)** of 19-week-old male *Rip.cre* mice and βRKO mice.

D) Absence of morphological changes in the pancreas of the βRKO mouse. Immunohistochemistry of serial pancreatic sections of 20-week-old *Rip.cre* mice and βRKO mice.

Bars represent means ± SE of n = 7–8 mice. Levels of significance (Student's t test) are shown (NS, not significant).

159 ± 15 mg/dl; p = 0.95; Figure 4B) or plasma insulin (βRKO, 2.78 ± 1.10 ng/ml versus *Rip.cre*, 2.67 ± 0.55 ng/ml; p = 0.92; Figure 4C) in the fed state. Hematoxylin-eosin (HE) staining and immunohistochemical studies with glucagon, insulin, Pdx1, somatostatin, PP, pan-CK, and amylase revealed no abnormalities (Figure 4D). These data indicate that Rbp-j is not required for maintaining β cell function or β cell mass.

Discussion

Using the stage-specific conditional gene targeting approach, we documented the effects of Notch/Rbp-j signaling on pancreatic development and function.

Normally, Ngn3 expression peaks between E13.5 and E15.5 (Apelqvist et al., 1999). In PRKO mice, Ngn3 expression peaked at E10.5 and then declined at E11.5 (Figure 1), which suggests that termination of Notch signaling results in earlier commitment to endocrine cell lineages and earlier loss of endocrine progenitor cells. Before E12.5, the majority of endocrine cells formed are α and PP cells, and a wave of β and δ cell generation occurs after E13 (Pictet and Rutter, 1972; Murtaugh and Melton, 2003). In PRKO mice, α and PP cell differentiation was enhanced at E11.5, but β and δ cell differentiation was not enhanced. It was recently reported that Ngn3 protein transduction to E11.5 pancreatic cells resulted in α cell differentiation, but the transduction to E15 cells resulted in β cell differentiation (Dominguez-Bendala et al., 2005). In agreement with that report, our findings suggest that E11 proendocrine cells may lack some factor that contributes to β or δ cell differentiation.

Tubular structures with CK^+ DBA^+ cells dominated in the pancreas of the PRKO mouse at later embryonic stages (Figure 2). Thus, residual $Pdx1^+$ epithelial cells that have not undergone endocrine cell differentiation have a tendency to differentiate into ductal cells. A study demonstrated that genes that participate in the Notch pathway are upregulated in the metaplastic ductal epithelium of pancreatic premalignant legions (Miyamoto et al., 2003). Lineage-tracing studies show that ductal lineage is separated from $Pdx1^+$ $Ngn3^-$ common pancreatic progenitor cells between E9.5 and E12.5 (Gu et al., 2002); those are the times when the disruption of *Rbp-j* genes in PRKO mice occurs. These findings suggest that the appropriate downregulation of Notch signaling is necessary for pancreatic duct cell identity.

In the mutant mouse, the number of Pdx1-positive cells clearly decreased before E15 and the pancreas was small thereafter (Figures 2B′, 3A, and 3B). If the role of Notch signaling is simply to regulate cell fate, hypoplasia of certain types of cell should be accompanied by hyperplasia of other types of cell. For instance, in the determination of T and B lymphocytes, loss of function of Notch1 resulted in blockade of T cell development and enhancement of B cell production, while overexpression of Notch1 resulted in blockade of B cell lymphopoiesis and the generation of T cells (Pui et al., 1999; Wilson et al., 2001). The small pancreas and altered pancreatic cell composition in our mutant mouse suggest that defective Notch signaling allows premature differentiation of α, PP, and duct cells at the expense of later differentiating β, δ, and acinar cells. This mode of regulation is reminiscent of neuronal differentiation, in which Notch/Rbp-j signaling acts as a gatekeeper between self-renewal and commitment (Ishibashi et al., 1995).

In PRKO mice, though inadequate, the differentiation and growth of acinar cells occurred after E15. Persistent Notch ICD expression in pancreatic epithelium has been shown to inhibit acinar cell differentiation (Hald et al., 2003; Esni et al., 2004), and generalized Hes1 KO mice showed increased acinar cell growth (Jensen et al., 2000a). These results also suggest that Notch signaling inhibits acinar cell differentiation and proliferation during later embryonic stages.

The role of Notch signaling in terminally differentiated cells is unknown, although it was speculated that Notch might confer some degree of plasticity on postmitotic neurons (Ahmad et al., 1995). We detected the expression of Notch2 and Dll1 in endocrine cells of adult mice (data not shown). Furthermore, $Ngn3^+$ endocrine progenitor cells were shown to reside within the pancreatic islets (Gu et al., 2002); however, we found no difference between βRKO mice and control mice (Figure 4). It was reported that the β cells in adult islets are mainly formed by self-duplication of preexisting β cells and that the forced expression of Notch1 ICD in the adult pancreas does not perturb mature endocrine cells (Murtaugh et al., 2003; Dor et al., 2004). Together with the results of PRKO mice, Notch signaling may be indispensable only during the early developmental stages of the pancreas.

Our data show that Rbp-j is a key molecule in the propagation of pancreatic progenitor cells and is essential for proper differentiation into mature pancreatic cells.

Experimental procedures

Generation of pancreas- or β cell-specific Rbp-j KO mice

The generations of mice bearing a floxed allele of *Rbp-j* have been described previously (Han et al., 2002). *Pdx.cre* mice in which Cre recombinase is under the transcriptional control of the mouse Pdx1 promoter were gifts from Dr. Douglas A. Melton (Gu et al., 2002). *Rip.cre* mice in which Cre recombinase is under the control of the rat insulin II promoter were purchased from the Jackson Laboratory. Mice homozygous for the floxed *Rbp-j* allele (F/F) were crossed with *Pdx.cre* or *Rip.cre* transgenic mice. The resultant double-heterozygous mice were then crossed with *Rbp-j*$^{f/+}$ mice, resulting in *Rbp-j*$^{f/f}$ *Pdx.cre* (PRKO) or *Rbp-j*$^{f/f}$ *Rip.cre* (βRKO) mice and their control littermates. Genotyping and assessment of deletion efficiency were performed by Southern blot analyses on genomic DNA obtained from tails or other tissues.

Histological analyses

Whole embryos or excised pancreas were fixed with 4% paraformaldehyde in PBS for overnight at 4°C then paraffin embedded, and 5 μm sections were cut and mounted on glass slides. Slides were dewaxed, rehydrated, and, in some instances, subjected to antigen retrieval by autoclaving at 121°C for five minutes with 10 mM citrate buffer. Endogenous peroxidase was inactivated with 0.3% H_2O_2 in methanol for 30 min. The slides were blocked for 1 hr with a reagent containing casein (DAKO Protein Block Serum-Free Solution; Dako), then stained overnight with the following primary antibodies (Abs): rabbit anti-Pdx1 (Guz et al., 1995), rabbit anti-Hes1 (Jensen et al., 2000a), rabbit anti-Ngn3 (Schwitzgebel et al., 2000), guinea pig anti-Insulin (Dako), rabbit anti-Glucagon (Dako), rabbit anti-Somatostatin (Dako), rabbit anti-PP (Dako), rabbit anti-Ghrelin (Kojima et al., 1999), rabbit anti-pHH3 (Cell Signaling Technology), rabbit anti-pan-CK (Santa Cruz), rabbit anti-Amylase (Sigma-Aldrich), rabbit anti-Glut2 (Thorens et al., 1992), mouse anti-ISL1 (Developmental Studies Hybridoma Bank). The slides were washed with PBS the following day and incubated for 2 hr with the following secondary antibodies: biotinylated goat anti-guinea pig IgG; biotinylated goat anti-rabbit IgG, and biotinylated rabbit anti-goat IgG (all from Vector). The slides were then incubated with avidin-biotin complex (ABC) reagent (Vectastain Elite ABC Kit; Vector) for 50 min followed by the addition of diaminobenzidine tetrahydrochloride (DAB) (Dako) as a substrate-chromogen solution. After hematoxylin counterstaining and dehydration, slides were mounted in mounting medium (MGK-S; Matsunami) and pictures were taken using an Axioskop Microscope (Carl Zeiss). Morphometric analyses of pancreas were carried out using the Scion Image analysis program (Scion). The number of islets was calculated, with the definition of an islet as a group of endocrine cells containing at least five visible nuclei. The endocrine cell mass was calculated as the ratio of each hormone-positive cell area to the total area of the pancreas section. An In situ Apoptosis Detection Kit (Takara) was used for TUNEL (terminal deoxynucleotidyl transferase-mediated dUTP nick end labeling) assays, and tissue taken from the involuting mammary gland of a post-lactating female Wistar rat was used as a positive control for apoptosis. Counterstaining of these sections was performed with methyl green. For E15 embryos, in situ hybridization of *Hes1* was carried out using digoxigenin-labeled cRNA probes according to the reported protocol (Tomita et al., 2000).

Analysis of metabolic parameters

Blood glucose values were determined from whole venous blood taken from mouse tails using an automatic glucometer (Glutest Ace, Sanwa Kagaku) or an enzyme colorimetric assay kit (Glucose CII test, Wako). Blood for insulin and amylase was taken by retroorbital bleeds. Plasma insulin levels were measured using an ELISA kit (Morinaga). For glucagon, blood samples were collected into tubes containing EDTA (1 mg/ml blood) and aprotinin (500 KIE/ml blood). For measurements of pancreatic insulin contents, pancreas were quickly dissected, weighed, and frozen in liquid nitrogen. Insulin was extracted by mechanical homogenization in iced acid ethanol. After 24 hr at 4°C, samples were centrifuged, and the supernatant was collected and stored at −20°C. Insulin concentrations were determined by ELISA. Amylase activity was measured according to the Caraway method using a kit (Amylase-Test Wako, Wako). All values are expressed as mean ± standard error.

Supplemental data

Supplemental Data include six figures, Supplemental Results, and Supplemental Experimental Procedures and can be found with this article online at http://www.cellmetabolism.org/cgi/content/full/3/1/59/DC1/.

Acknowledgments

We thank Dr. Douglas A. Melton for providing *Pdx.cre* mice, Dr. Christopher V.E. Wright for anti-Pdx1 Ab, Dr. Michael S. German for anti-Ngn3 Ab, Dr. Bernard Thorens for anti-Glut2 Ab, Dr. Kenji Kangawa for anti-Ghrelin Ab, and Ryoichiro Kageyama for anti-Hes1 Ab. This work was supported by research grants from the Japanese Ministry of Education, Culture, Sports, Science, and Technology and the Japanese Ministry of Health, Labor and Welfare.

Received: August 2, 2005
Revised: October 30, 2005
Accepted: December 16, 2005
Published: January 10, 2006

References

Ahlgren, U., Pfaff, S.L., Jessell, T.M., Edlund, T., and Edlund, H. (1997). Independent requirement for ISL1 in formation of pancreatic mesenchyme and islet cells. Nature *385*, 257–260.

Ahmad, I., Zaqouras, P., and Artavanis-Tsakonas, S. (1995). Involvement of Notch-1 in mammalian retinal neurogenesis: association of Notch-1 activity with both immature and terminally differentiated cells. Mech. Dev. *53*, 73–85.

Apelqvist, A., Li, H., Sommer, L., Beatus, P., Anderson, D.J., Honjo, T., Hrabe de Angelis, M., Lendahl, U., and Edlund, H. (1999). Notch signalling controls pancreatic cell differentiation. Nature *400*, 877–881.

Dominguez-Bendala, J., Klein, D., Ribeiro, M., Ricordi, C., Inverardi, L., Pastori, R., and Edlund, H. (2005). TAT-mediated neurogenin 3 protein transduction stimulates pancreatic endocrine differentiation in vitro. Diabetes *54*, 720–726.

Dor, Y., Brown, J., Martinez, O.I., and Melton, D.A. (2004). Adult pancreatic beta-cells are formed by self-duplication rather than stem-cell differentiation. Nature *429*, 41–46.

Esni, F., Ghosh, B., Biankin, A.V., Lin, J.W., Albert, M.A., Yu, X., MacDonald, R.J., Civin, C.I., Real, F.X., Pack, M.A., et al. (2004). Notch inhibits Ptf1 function and acinar cell differentiation in developing mouse and zebrafish pancreas. Development *131*, 4213–4224.

Gradwohl, G., Dierich, A., LeMeur, M., and Guillemot, F. (2000). Neurogenin3 is required for the development of the four endocrine cell lineages of the pancreas. Proc. Natl. Acad. Sci. USA *97*, 1607–1611.

Gu, G., Dubauskaite, J., and Melton, D.A. (2002). Direct evidence for the pancreatic lineage: NGN3+ cells are islet progenitors and are distinct from duct progenitors. Development *129*, 2447–2457.

Guz, Y., Montminy, M.R., Stein, R., Leonard, J., Gamer, L.W., Wright, C.V.E., and Teitelman, G. (1995). Expression of murine STF-1, a putative insulin gene transcription factor, in β cells of pancreas, duodenal epithelium and pancreatic exocrine and endocrine progenitors during ontogeny. Development *121*, 11–18.

Hald, J., Hjorth, J.P., German, M.S., Madsen, O.D., Serup, P., and Jensen, J. (2003). Activated Notch1 prevents differentiation of pancreatic acinar cells and attenuate endocrine development. Dev. Biol. *260*, 426–437.

Hamada, Y., Kadokawa, Y., Okabe, M., Ikawa, M., Coleman, J.R., and Tsujimoto, Y. (1999). Mutation in ankyrin repeats of the mouse Notch2 gene induces early embryonic lethality. Development *126*, 3415–3424.

Han, H., Tanigaki, K., Yamamoto, N., Kuroda, K., Yoshimoto, M., Nakahata, T., Ikuta, K., and Honjo, T. (2002). Inducible gene knockout of transcription factor recombination signal binding protein-J reveals its essential role in T versus B lineage decision. Int. Immunol. *14*, 637–645.

Heller, R.S., Jenny, M., Collombat, P., Mansouri, A., Tomasetto, C., Madsen, O.D., Mellitzer, G., Gradwohl, G., and Serup, P. (2005). Genetic determinants of pancreatic epsilon-cell development. Dev. Biol. *286*, 217–224.

Hrabé de Angelis, M., McIntyre, J., II, and Gossler, A. (1997). Maintenance of somite borders in mice requires the Delta homologue Dll1. Nature *386*, 717–721.

Ishibashi, M., Ang, S.L., Shiota, K., Nakanishi, S., Kageyama, R., and Guillemot, F. (1995). Targeted disruption of mammalian hairy and Enhancer of split homolog-1 (HES-1) leads to up-regulation of neural helix-loop-helix factors, premature neurogenesis, and severe neural tube defects. Genes Dev. *9*, 3136–3148.

Jensen, J., Pedersen, E.E., Galante, P., Hald, J., Heller, R.S., Ishibashi, M., Kageyama, R., Guillemot, F., Serup, P., and Madsen, O.D. (2000a). Control of endodermal endocrine development by Hes-1. Nat. Genet. *24*, 36–44.

Jensen, J., Heller, R.S., Funder-Nielsen, T., Pedersen, E.E., Lindsell, C., Weinmaster, G., Madsen, O.D., and Serup, P. (2000b). Independent development of pancreatic alpha- and beta-cells from neurogenin3-expressing precursors: a role for the notch pathway in repression of premature differentiation. Diabetes *49*, 163–176.

Kageyama, R., and Ohtsuka, T. (1999). The Notch-Hes pathway in mammalian neural development. Cell Res. *9*, 179–188.

Kato, H., Sakai, T., Tamura, K., Minoguchi, S., Shirayoshi, Y., Hamada, Y., Tsujimoto, Y., and Honjo, T. (1996). Functional conservation of mouse Notch receptor family members. FEBS Lett. *395*, 221–224.

Kojima, M., Hosoda, H., Date, Y., Nakazato, M., Matsuo, H., and Kangawa, K. (1999). Ghrelin is a growth-hormone-releasing acylated peptide from stomach. Nature *402*, 656–660.

Lammert, E., Brown, J., and Melton, D.A. (2000). Notch gene expression during pancreatic organogenesis. Mech. Dev. *94*, 199–203.

Miyamoto, Y., Maitra, A., Ghosh, B., Zechner, U., Argani, P., Iacobuzio-Donahue, C.A., Sriuranpong, V., Iso, T., Meszoely, I.M., Wolfe, M.S., et al. (2003). Notch mediates TGF alpha-induced changes in epithelial differentiation during pancreatic tumorigenesis. Cancer Cell *6*, 565–576.

Murtaugh, L.C., and Melton, D.A. (2003). Genes, signals, and lineages in pancreas development. Annu. Rev. Cell Dev. Biol. *19*, 71–89.

Murtaugh, L.C., Stanger, B.Z., Kwan, K.M., and Melton, D.A. (2003). Notch signaling controls multiple steps of pancreatic differentiation. Proc. Natl. Acad. Sci. USA *100*, 14920–14925.

Oka, C., Nakano, T., Wakeham, A., de la Pompa, J.L., Mori, C., Sakai, T., Okazaki, S., Kawaichi, M., Shiota, K., Mak, T.W., and Honjo, T. (1995). Disruption of the mouse RBP-J kappa gene results in early embryonic death. Development *121*, 3291–3301.

Pang, K., Mukonoweshuro, C., and Wong, G.G. (1994). Beta cells arise from glucose transporter type 2 (Glut2)-expressing epithelial cells of the developing rat pancreas. Proc. Natl. Acad. Sci. USA *91*, 9559–9563.

Pictet, R., and Rutter, W.J. (1972). Development of the embryonic endocrine pancreas. In Handbook of Physiology, Section *7*, D.F. Steiner and N. Frenkel, eds. (Baltimore, MD: Williams and Williams), pp. 25–66.

Pui, J.C., Allman, D., Xu, L., DeRocco, S., Karnell, F.G., Bakkour, S., Lee, J.Y., Kadesch, T., Hardy, R.R., Aster, J.C., and Pear, W.S. (1999). Notch1 expression in early lymphopoiesis influences B versus T lineage determination. Immunity *11*, 299–308.

Schwitzgebel, V.M., Scheel, D.W., Conners, J.R., Kalamaras, J., Lee, J.E., Anderson, D.J., Sussel, L., Johnson, J.D., and German, M.S. (2000). Expression of neurogenin3 reveals an islet cell precursor population in the pancreas. Development *127*, 3533–3542.

Swiatek, P.J., Lindsell, C.E., del Amo, F.F., Weinmaster, G., and Gridley, T. (1994). Notch1 is essential for postimplantation development in mice. Genes Dev. *15*, 707–719.

Thorens, B., Wu, Y.J., Leahy, J.L., and Weir, G.C. (1992). The loss of GLUT2 expression by glucose-unresponsive cells of db/db mice is reversible and is induced by the diabetic environment. J. Clin. Invest. *90*, 77–85.

Tomita, K., Moriyoshi, K., Nakanishi, S., Guillemot, F., and Kageyama, R. (2000). Mammalian achaete-scute and atonal homologs regulate neuronal versus glial fate determination in the central nervous system. EMBO J. *19*, 5460–5472.

Wilson, A., MacDonald, H.R., and Radtke, F. (2001). Notch 1-deficient common lymphoid precursors adopt a B cell fate in the thymus. J. Exp. Med. *194*, 1003–1012.

Xue, Y., Gao, X., Lindsell, C.E., Norton, C.R., Chang, B., Hicks, C., Gendron-Maguire, M., Rand, B., Weinmaster, G., and Gridley, T. (1999). Embryonic lethality and vascular defects in mice lacking the Notch ligand Jagged1. Hum. Mol. Genet. *8*, 723–730.

0013-7227/06/$15.00/0
Printed in U.S.A.

Endocrinology 147(4):1642–1653

doi: 10.1210/en.2005-1038

The Neuroprotective and Vasculo-Neuro-Regenerative Roles of Adrenomedullin in Ischemic Brain and Its Therapeutic Potential

Kazutoshi Miyashita, Hiroshi Itoh, Hiroshi Arai, Takayasu Suganami, Naoki Sawada, Yasutomo Fukunaga, Masakatsu Sone, Kenichi Yamahara, Takami Yurugi-Kobayashi, Kwijun Park, Naofumi Oyamada, Naoya Sawada, Daisuke Taura, Hirokazu Tsujimoto, Ting-Hsing Chao, Naohisa Tamura, Masashi Mukoyama, and Kazuwa Nakao

Department of Medicine and Clinical Science (K.M., H.I., H.A., N.S., Y.F., M.S., K.Y., T.Y.-K., K.P., N.O., N.S., D.T., H.T., N.T., M.M., K.N.), Kyoto University Graduate School of Medicine, Kyoto 606-8507, Japan; Department of Molecular Medicine and Metabolism (T.S.), Medical Research Institute, Tokyo Medical and Dental University, Tokyo 101-0062, Japan; and Department of Medicine (T.-H.C.), National Cheng-Kung University Medical Center, Tainan, Taiwan 701, Republic of China

Adrenomedullin (AM) is a vasodilating hormone secreted mainly from vascular wall, and its expression is markedly enhanced after stroke. We have revealed that AM promotes not only vasodilation but also vascular regeneration. In this study, we focused on the roles of AM in the ischemic brain and examined its therapeutic potential. We developed novel AM-transgenic (AM-Tg) mice that overproduce AM in the liver and performed middle cerebral artery occlusion for 20 min (20m-MCAO) to examine the effects of AM on degenerative or regenerative processes in ischemic brain. The infarct area and gliosis after 20m-MCAO was reduced in AM-Tg mice in association with suppression of leukocyte infiltration, oxidative stress, and apoptosis in the ischemic core. In addition, vascular regeneration and subsequent neurogenesis were enhanced in AM-Tg mice, preceded by increase in mobilization of CD34$^+$ mononuclear cells, which can differentiate into endothelial cells. The vasculo-neuro-regenerative actions observed in AM-Tg mice in combination with neuroprotection resulted in improved recovery of motor function. Brain edema was also significantly reduced in AM-Tg mice via suppression of vascular permeability. *In vitro*, AM exerted direct antiapoptotic and neurogenic actions on neuronal cells. Exogenous administration of AM in mice after 20m-MCAO also reduced the infarct area, and promoted vascular regeneration and functional recovery. In summary, this study suggests the neuroprotective and vasculo-neuro-regenerative roles of AM and provides basis for a new strategy to rescue ischemic brain through its multiple hormonal actions. (*Endocrinology* 147: 1642–1653, 2006)

ADRENOMEDULLIN (AM) IS a potent vasodilating peptide comprising 52 amino acids, which was originally isolated from human pheochromocytoma tissues in 1993 as a substance to elevate cAMP concentration in platelets (1). It is secreted mainly from the vascular wall into circulating blood to reduce pre- and post-load on the heart via vasodilation, natriuresis, and suppression of aldosterone release. Intravenous administration of AM to patients with heart failure or pulmonary hypertension has already been initiated and beneficial hemodynamic effects have been reported (2).

First Published Online December 29, 2005

Abbreviations: AM, Adrenomedullin; ANCOVA, analysis of covariance; BP, blood pressure; BrdU, bromodeoxyuridine; CGRP, calcitonin gene-related peptide; diHE, dihydroethidium; GFAP, glial fibrillary acidic protein; LDPI, laser Doppler perfusion imager; MCA, middle cerebral artery; 20m-MCAO, middle cerebral artery occlusion for 20 min; NeuN, neuronal marker; NHNP, normal human neuronal progenitor cells; PAMP, proadrenomedullin N-terminal 20 peptide; PECAM, platelet endothelial cell adhesion molecule; PI3K, phosphatidyl inositol-3 kinase; PKA, protein kinase A; ROS, reactive oxygen species; ssDNA, single-strand DNA; Tg, transgenic; Wt, wild type.

Endocrinology **is published monthly by The Endocrine Society (http://www.endo-society.org), the foremost professional society serving the endocrine community.**

Along with its vasodilating effect, a number of studies have demonstrated various and significant effects of AM on the regulation of vascular structure, including its development, remodeling, and regeneration. Mice lacking the AM gene did not survive their embryonic stage and showed abnormal vasculature with sc hemorrhage (3, 4). Mice overexpressing AM in endothelial cells were revealed to be hypotensive and resistant to vascular remodeling such as neointima formation caused by cuff injury, and atherogenesis associated with a high-cholesterol diet (5). We have recently established that AM promotes endothelial regeneration in the wound healing assay using cultured endothelial cells and enhances neovascularization *in vivo* into sc implanted gelplugs in mice (6, 7). We and others (8–11) have further demonstrated that the potentiating action of AM on vascular regeneration is mediated by activation of the phosphatidyl inositol-3 kinase (PI3K)-Akt pathway.

Recently, it has been known that AM is secreted from various organs including the heart, lung, kidney, adipose tissues, and central nervous system (12). Moreover, AM expression has been demonstrated to be markedly enhanced by ischemia through the activation of hypoxia-responsive elements in the AM gene via transcription factor hypoxia-inducible factor-1. In the central nervous system, where AM is

mainly expressed in neurons and the endothelium (13), it is reported that transient ischemia boosted AM expression for more than 15 d (14). However, the role of augmented AM has remained unclear for inconsistent previous results: three studies reported neuroprotective effects of AM by demonstrating reduction of infarct size after transient ischemia (15–17), whereas one study detected exacerbation of infarction as a result of AM infusion (14).

In this context, our study presented here focused on the roles of augmented AM in ischemic brain and examined its therapeutic potential. We generated new lines of transgenic mice that overproduce AM (AM-Tg) in the liver that mimics chronic AM administration. After inducing 20-min middle cerebral artery occlusion (20m-MCAO) to produce a nonfatal stroke model in the AM-Tg mice, we observed the long-term effects of AM on the ischemic brain up to postoperative d 56. We examined the mice for the recovery of blood flow in the ischemic region and impaired motor function after stroke, and immunohistochemically examined the ischemic striatum to determine effects of AM on neuronal loss/apoptosis, gliosis, leukocyte infiltration, oxidative stress, vascular regeneration, and neurogenesis after 20m-MCAO. In addition, another stroke model, 2-h middle cerebral artery occlusion (2 h-MCAO), was performed to observe the effect of AM in acute phase of the fatal stroke. *In vitro* studies using neuronal progenitor cells or rat pheochromocytoma PC12 cells were performed to examine direct antiapoptotic and neurogenic actions of AM on these neuronal cells. Finally, we investigated the effect of exogenous AM administration after 20m-MCAO to determine the appropriate amount and timing of AM treatment after cerebral ischemia.

Materials and Methods

Generation of transgenic mice which overproduce human AM but do not overproduce mature proadrenomedullin N-terminal 20 peptide (PAMP)

The AM gene contains coding regions for not only AM but also PAMP, a different vasodilating peptide. Amidation at their carboxyl terminals after their synthesis is needed for both AM and PAMP to exert their biological activity. The bioactive amidated forms are known as mature AM and mature PAMP, respectively. To identify the specific effects of AM, we generated a transgene construct with a point mutation on the PAMP amidation signal in the full-length AM gene cDNA. Guanine was substituted for cytosine on the 3′ end of the PAMP coding region so that glycine on the C′ terminal of the PAMP product was replaced with alanine. In this way, amidation and maturation of PAMP by peptidylglycine α-hydroxylase and α-hydroxyglycine N-C lyase were inhibited (Fig. 1A). The mutant AM gene cDNA was then inserted into a plasmid containing the human serum amyloid P component promoter, which is widely used to target gene expression specific to the liver. When the product is secreted from the liver, it mimics intravenous administration of the agent. The *Hin*dIII-*Xho*I fragment of the plasmid was microinjected into the pronucleus of fertilized C57BL/6J mice eggs.

The copy number of transgenes was quantified by means of genomic Southern blotting according to standard procedure. Plasma concentrations of human total AM and mature AM were measured with a commercially available immunoradiometric assay (Cosmic, Tokyo, Japan).

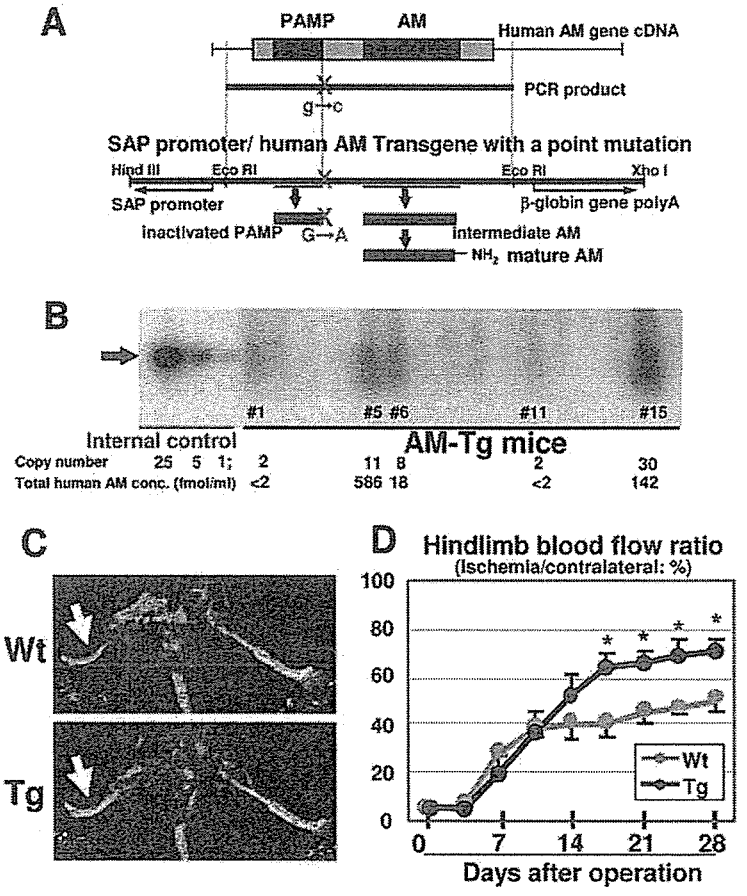

FIG. 1. Generation of transgenic mice which overproduce AM but do not overproduce mature PAMP in the liver and augmented angiogenesis in the transgenic mice after femoral artery occlusion. A, Schematic representation of the transgene construct derived from human AM gene cDNA with a point mutation in the amidation signal of PAMP. B, Southern blot analysis of the tail DNA of the founder mice. *Arrow*, Blots for the transgene. Internal controls for indicated copies are located in the *left three lanes*. The line No. indicates the mice in which the transgene was detected by PCR. The copy numbers estimated by densitometry and the plasma concentrations of total human AM in F3 mice of the lines are shown. C, Hindlimb blood flow analyzed by LDPI. *Red* or *white* indicates a higher flow than *blue* or *green*. *Arrows*, Comparison of ischemic hindlimbs between Wt and AM-Tg on d 28 after femoral artery ligation. D, Quantitative analysis of the hindlimb blood flow in ischemia. *, $P < 0.05$ for Wt *vs.* AM-Tg by ANCOVA; n = 6.

Human mature PAMP concentration was measured with a recently developed enzyme immunoassay (18). To determine the brain concentration of AM, we used the RIA kits for measurement of human and mouse total AM (Phoenix, Belmont, CA), according to the manufacturer's instruction. Blood pressure (BP) was measured with tail cuff (Softron, Tokyo, Japan). Hindlimb ischemia was induced by ligating the right femoral artery and blood flow of the ischemic limb was estimated with a laser Doppler perfusion imager (LDPI; Moor Instruments Ltd., Devon, UK) to confirm the angiogenic effect of AM-Tg mice. The perfusion ratio (%) was calculated as that of the ipsilatereal to the contralateral side. Animal care and experiments were in accordance with the guidelines for animal experiments of Kyoto University.

Induction of stroke by MCAO

We performed nonfatal 20m-MCAO and fatal 2 h-MCAO by the standard *trans*-luminal method, which has been described in various previous reports (19). Briefly, a 8–0 nylon monofilament coated with silicone was inserted from the left common carotid artery via the internal carotid to the base of the left middle cerebral artery (MCA) of 12-wk-old mice anesthetized with 5% halothane and maintained on 1%. After 20 min or 2 h of occlusion, the filament was withdrawn; and the arteries were reperfused, whereas the left common carotid artery was permanently ligated. Occlusion and reperfusion of the MCA was confirmed by means of fiber-shaped laser Doppler perfusion imager (Omegawave, Tokyo, Japan). We observed the mice until postoperative d 56 to examine blood flow in the ischemic region with an LDPI and motor function with a rota-rod exercise test.

Immunohistochemical examination of the ischemic striatum

After the induction of 20m-MCAO, mice were killed on postoperative d 0–56 and the harvested brains were subjected to immunohistochemical examination using a standard procedure described elsewhere (20). We used these primary antibodies: neuronal marker, NeuN (1:200; Chemi-Con, Temecula, CA); astrocyte marker, glial fibrillary acidic protein (GFAP) (1:400; Chemicon); apoptosis marker, single-strand DNA (ssDNA) (1:50; Dako, Carpinteria, CA); leukocyte marker, CD45 (1:100, PharMingen, San Diego, CA); endothelial marker, platelet endothelial cell adhesion molecule (PECAM)-1 (CD31) (1:100, PharMingen); and a marker for proliferating cells, bromodeoxyuridine (BrdU) (1:50, Molecular Probes, Eugene, OR); to examine infarct area, gliosis, leukocyte infiltration, apoptosis, vascular regeneration and neurogenesis. Briefly, free-floating 30-μm coronal sections at the level of the anterior commissure were stained and observed with a confocal microscope (LSM5 PASCAL; Carl Zeiss SMT AG, Oberkochen, Germany). The infarct area (mm^2/field) was defined and quantified as the region where loss of NeuN immunoreactivity was observed and gliosis (mm^2/field) as the area stained GFAP in the ischemic striatum at × 5 fields. CD45 or ssDNA-positive cells (cells/mm^2) were quantified to serve as an index of leukocyte infiltration or of apoptosis, respectively, in the ischemic core at ×20 magnification. Capillary density was quantified as the number of PECAM-1-positive cells (cells/mm^2). The vessel counts were performed in the region of ischemic core at 0.5~1.0 mm anterior from the bregma. We prepared two thin sections (6 μm thickness) per mouse for vessel counting and four representative fields from each section were evaluated for capillary density in the ischemic core. To examine neurogenesis, mice were injected ip with BrdU 50 mg/kg (Sigma-Aldrich Co., St. Louis, MO) twice daily on postoperative d 4–6 and the number of BrdU-NeuN double-positive cells (cells/mm^2), which are generally defined as regenerated neurons, were quantified to serve as an index of neurogenesis. We also examined the production of reactive oxygen species (ROS) *in situ* by using the oxidative fluorescent dye dihydroethidium (diHE; 2×10^{-6} M; Sigma).

Quantification of CD34$^+$ mononuclear cells after 20m-MCAO

We counted peripheral $CD34^+$ mononuclear cells according to the International Society of Hematotherapy and Graft Engineering (ISHAGE) guidelines (21). Briefly, peripheral blood was taken from the orbital vein and stained with CD34-PE and CD45-FITC monoclonal antibodies (BD PharMingen, San Jose, CA) in a TruCOUNT tube (BD PharMingen) according to the manufacturer's instruction. After the reaction, $CD34^+$-$CD45^{dim}$ cells were quantified as $CD34^+$ mononuclear cells by a fluorescence-activated cell sorting machine Aria (BD) by using the ISHAGE sequential gating strategy (21).

Analysis of infarct volume and brain edema after 2 h-MCAO

We performed 2 h-MCAO to examine the effect of AM in the acute phase of fatal stroke. To estimate infarct or edema volume, mice were killed 24 h after the occlusion. The brain was removed and cut into 2 mm-thick slices and immersed in saline containing 2% 2,3,5-triphenyltetrazolium chloride for 30 min at 4 C. Infarct or edema volume was calculated as the percentage volume of the contralateral hemisphere with a standard procedure as described elsewhere (22). We estimated Evans Blue leakage in the brain parenchyma as previously reported (23), to serve as an index of vascular permeability *in situ*. Briefly, 0.2 ml of 2.5% Evans Blue solution was injected into mice via a tail vein 10 min before 2 h-MCAO and mice were killed at 24 h after the ischemia. Brain tissues were weighed and homogenized in 50% trichloroacetic acid solution to extract the dye in the supernatant. The tissue content of Evans Blue was estimated from the absorbance of 620 nM.

Estimation of apoptosis and differentiation of neuronal cells

The ratio of apoptotic cells was examined using normal human neuronal progenitor cells (NHNP; Cambrex Bioscience, Walkersville, MD). Cells were plated at a density of 5×10^4 cells/cm^2 on a laminin-coated 24-well dish and incubated in serum-free neuronal basal medium for 48 h. After the experimental period, the cell number was assessed by 5-mercapto-1-methyltetrazole assay (Nakalai Tesque), and the cells were stained with an anti-ssDNA antibody and nuclear staining propidium iodide to calculate the ratio of apoptotic cells to the total cells in each microscopic image.

Neuronal differentiation was examined as described previously (24), using rat pheochromocytoma PC12 cells (Riken Gene Bank, Tsukuba, Japan). Briefly, the length of the neuronal process (micrometers/cell) was calculated to serve as an index of neuronal differentiation after plating at a density of 10^4 cells/cm^2 on a collagen I-coated 24-well dish and incubated in 1% serum DMEM for 7 d. The cells were treated with 10^{-5}mol/liter AM or 100 ng/ml nerve growth factor as a positive control, and with the following inhibitors: the two AM antagonists, 10^{-5}mol/liter AM (22–52) and 10^{-5} mol/liter calcitonin gene-related peptide(8–37) [CGRP(8–37)] (Peptide Institute Inc., Osaka, Japan), the two protein kinase A (PKA) inhibitors, 10^{-5} mol/liter adenosine 3P,5P-cyclic monophosphorothioate Rp-isomer (Rp-cAMP) and 10^{-6} mol/liter myristoylated cell-permeable PKA inhibitor peptide sequence (14–22) (PKA Inh), and the two PI3K inhibitors, 10^{-5} mol/liter LY294002 and 10^{-7} mol/liter wortmannin (Calbiochem, San Diego, CA). For endothelial cell coculture experiments, human umbilical vein endothelial cells (HUVEC; Cambrex) were plated into transwell membrane inserts at a density of 10^5 cells/cm^2.

Exogenous administration of AM and hydralazine

Recombinant human mature AM dissolved in 0.9% saline was exogenously administrated to C57BL/6J wild-type mice (Wt) by means of osmotic pumps (Alzet Model 2002; Alzet Osmotic Pumps Co., Cupertino, CA) at a rate of 50 ng/h, which is estimated to achieve a plasma concentration of 2 fmol/ml (25). To determine appropriate timing to start AM treatment after 20m-MCAO, we implanted the pump ip just after the operation (d 0), or at 24 (d 1) or 72 h (d 3) later. We killed the mice on d 7 for histological examination and the period of the exogenous AM treatment was from d 0, 1, or 3 to d 7. In some experiments, low-dose (0.1 mM) hydralazine was exogenously administrated in drinking water.

Statistics

All data were expressed as mean ± SE. Comparison of means between two groups was performed with Student's *t* test. When more than two groups were compared, ANOVA was used to evaluate significant differences among groups, and if significant differences were confirmed, each difference was further examined by means of multiple comparisons. We

TABLE 1. Plasma concentrations of human AM and systolic BP in Wt and three lines of AM-Tg mice

	Wt	Low conc.	Medium conc.	High conc.
Total AM (fmol/ml)	1.1 ± 0.2	17.6 ± 4.4[a]	142.2 ± 18.4[a]	585.5 ± 117.7[a]
Mature AM (fmol/ml)	0.5 ± 0.4	2.6 ± 0.6[a]	10.4 ± 2.4[a]	24.9 ± 4.2[a]
Systolic BP (mm Hg)	122.7 ± 1.6	113.0 ± 2.5[a]	113.4 ± 2.6[a]	109.4 ± 2.5[a]

conc., Concentration.
[a] $P < 0.01$ *vs.* Wt; n = 4–12.

performed analysis of covariance (ANCOVA) when repeated-measurement had done, specifically, in the rota-rod test and laser Doppler flowmetry. Probability was considered to be statistically significant at $P < 0.05$.

Results

Generation of transgenic mice that overproduce human AM but do not overproduce mature PAMP

We generated seven lines of founder mice carrying the transgene and maintained three of them (lines 5, 6, and 15). Their plasma concentrations of human total AM were 585.5 ± 117.7, 17.6 ± 4.4 and 142.2 ± 18.4 fmol/ml and the copy numbers of the transgene estimated by Southern blot densitometry analysis were 11, 8, and 30, respectively (Fig. 1B). The physiological concentration of mouse total AM is reportedly 5~10 fmol/ml, so that the transgenic mice were expected to overproduce AM about 100, 3, and 30 times more than endogenous AM. The three lines were designated low (no. 6), medium (no. 15), and high (no. 5) concentration line according to their plasma AM concentration. The high concentration line (no. 5) was used for further study unless otherwise indicated. The plasma concentration of human mature AM, the bioactive amidated form, increased to 2.6~24.9 fmol/ml in the AM-Tg mice (Table 1). On the other hand, plasma human mature PAMP did not change in AM-Tg mice. The concentration (fmol/ml) was 2.21 ± 0.58 in Wt *vs.* 2.15 ± 0.35 in AM-Tg (n = 6), so that the point mutation on the amidation signal in the PAMP coding region was expected to successfully inhibit maturation of PAMP. There were no apparent differences in overall appearance, behavior, growth or fertility between Wt and AM-Tg mice. The systolic BP in 12-wk-old mice was significantly reduced in all three lines of AM-Tg compared with Wt. The BP (mm Hg) was 122.7 ± 1.6 in Wt *vs.* 109.4 ± 2.5~113.4 ± 2.6 in AM-Tg, depending on the line ($P < 0.05$; n = 5; Table 1).

Therapeutic angiogenesis in hindlimb ischemia model was promoted in AM-Tg mice

The recovery of blood flow in the ischemic hindlimb of Wt and AM-Tg mice was compared and was found to have

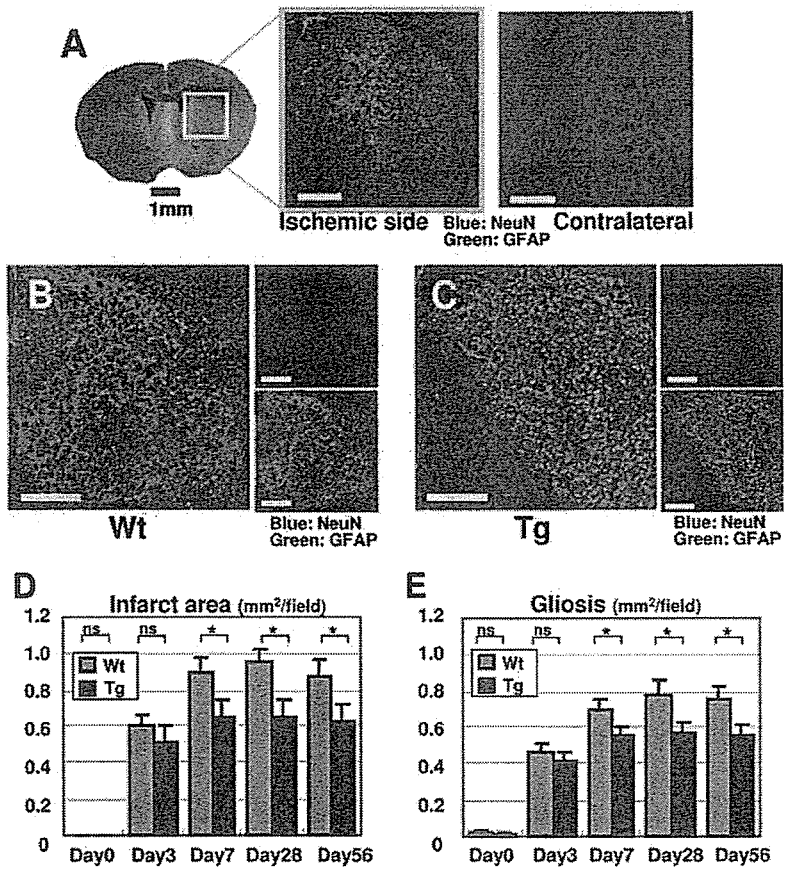

FIG. 2. Effects of AM on infarct area and gliosis after the nonfatal stroke, 20m-MCAO. A, Histological examination of the ischemic striatum. The outlined field was examined for infarct area and gliosis. The ischemic side and contralateral side on d 3 after 20m-MCAO are shown. *Scale bar*, 500 μm (×5 magnification). B and C, Representative images of the ischemic striatum on postoperative d 7 stained for NeuN (*blue*) and GFAP (*green*). Infarct area, defined as the region where NeuN immunoreactivity was lost, and gliosis, defined as the area where GFAP immunoreactivity was observed, in Wt (B) and AM-Tg (C) are shown. *Scale bar*, 500 μm (×5 magnification) D and E, Quantitative analysis of the infarct area (D) and gliosis (E) *, $P < 0.05$; ns, not significant for Wt *vs.* AM-Tg; n = 12.

significantly improved in AM-Tg mice after postoperative d 17. The hindlimb blood flow ratio on d 28 (ipsilateral/contralateral, %) was 56.6 ± 8.3 in Wt *vs.* 73.8 ± 5.3 in AM-Tg ($P < 0.05$; n = 6; Fig. 1, C and D). In this way, promotion of therapeutic angiogenesis by AM was confirmed in AM-Tg mice.

Brain remodeling in ischemic striatum after 20m-MCAO

We investigated the time course of neuronal loss, reactive gliosis, vascular regeneration, and neuronal regeneration; the entire process can be defined as "brain remodeling" after ischemia.

20m-MCAO caused selective loss of NeuN-positive cells and marked reactive gliosis (Fig. 2A) in the ipsilateral striatum within 24 h after the operation; this condition was different from pan-necrosis caused by longer MCAO (*e.g.* 2 h-MCAO). The infarct area, that is, the area of neuronal loss, expanded progressively up to d 7, and then showed gradual increase in size until d 56, whereas gliosis spread in parallel. The expansion of the infarct area in the subacute to chronic phase after mild stroke was compatible with previously reported findings (26). Vascular regeneration in the striatum with enhanced capillary density was obvious after postoperative d 7, and subsequent neurogenesis became obvious after d 28.

The concentrations of the overproduced human AM (fmol/g tissue) in the ischemic brain of AM-Tg mice before and on postoperative d 1 and 28 after 20m-MCAO were 27.8 ± 10.3, 87.4 ± 4.0 and 30.3 ± 16.8, respectively. Those of endogenous mouse AM (fmol/g tissue) were 3.7 ± 2.1, 7.2 ± 2.5, and 4.6 ± 3.0.

Infarct area and gliosis were reduced in AM-Tg mice after 20m-MCAO along with suppression of leukocyte infiltration and ROS production

A significant decrease in infarct area and gliosis was observed in AM-Tg mice (Fig. 2, B–E) after postoperative d 7, but was not obvious on d 3. The infarct area (mm^2/field) on d 56 was 0.88 ± 0.08 in Wt *vs.* 0.64 ± 0.08 in AM-Tg ($P < 0.05$; n = 12; Fig. 2D), and gliosis (mm^2/field) on the same day was 0.76 ± 0.08 in Wt and 0.56 ± 0.07 in AM-Tg ($P < 0.05$; n = 12; Fig. 2E). Leukocyte infiltration quantified as the number of $CD45^+$ cells was significantly suppressed in AM-Tg mice especially from d 3–7. $CD45^+$ cells on d 3 (/mm^2) numbered 197.5 ± 16.6 in Wt *vs.* 140.7 ± 14.6 in AM-Tg ($P < 0.05$; n = 12; Fig. 3, A, B, and G). *In situ* ROS production detected by immunostaining for diHE, which stained the nucleus of $NeuN^+$ or $GFAP^+$ cells, was enhanced in Wt compared with that in AM-Tg mice (Fig. 3, C and D). Apoptotic cells quantified as the number of $ssDNA^+$ cells in the ischemic core were significantly reduced in the AM-Tg mice on d 3–7. $ssDNA^+$ cells (/mm^2) on d 3 numbered 214.8 ± 19.6 in Wt *vs.* 123.2 ± 11.1 in AM-Tg ($P < 0.01$; n = 12; Fig. 3, E, F, and H).

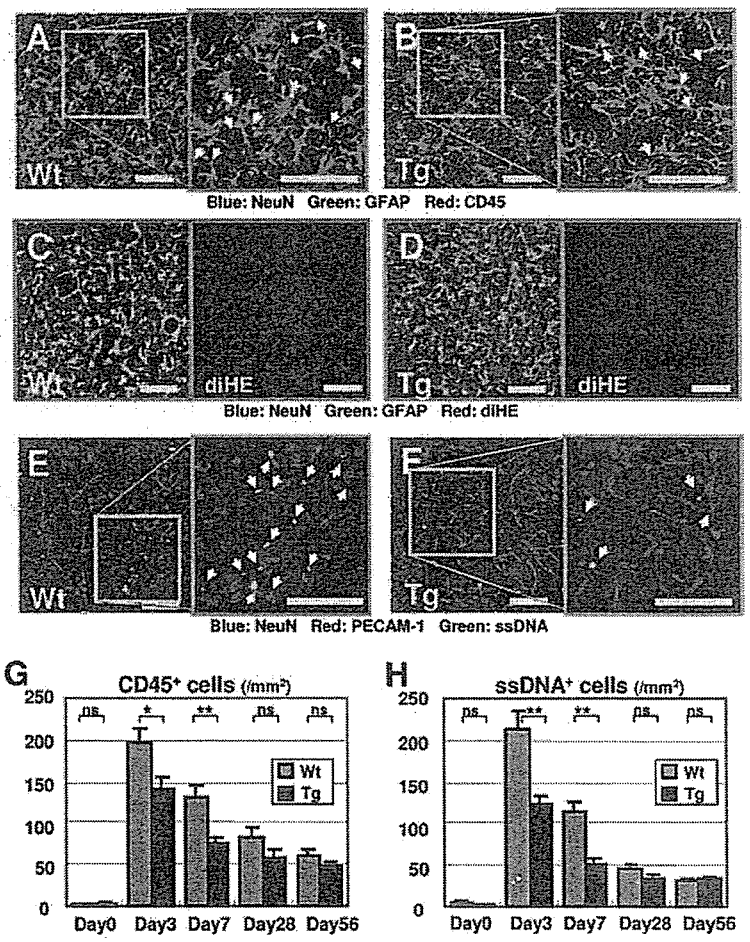

FIG. 3. Effects of AM on leukocyte infiltration, ROS production, and apoptosis in the ischemic brain after 20m-MCAO. A and B, Detection of leukocyte infiltration in the ischemic core on postoperative d 7 by immunostaining for $CD45^+$ cells (*red*) in Wt (A) and AM-Tg (B). *Arrows*, $CD45^+$ cells. C and D, *In situ* detection of ROS in ischemic striatum on postoperative d 7 by immunostaining for diHE (*red*) in Wt (C) and AM-Tg (D). E and F, Detection of apoptotic cells in the ischemic core on postoperative d 7 by immunostaining for $ssDNA^+$ cells (*green*) in Wt (E) and AM-Tg (F). *Arrows*, $ssDNA^+$ cells. G and H, Quantitative analysis of $CD45^+$ cells (G) and $ssDNA^+$ cells (H) in the ischemic core. *, $P < 0.05$; **, $P < 0.01$; ns, not significant for Wt *vs.* AM-Tg; n = 12. *Scale bar*, 100 μm (×20 magnification).